CFD Analysis of Iodine Mass Transfer Coupled with a Chemical Reaction in a Filtered Containment Venting System

By

Muhammad Shummas Humayun

Reg # 00000330307

Session 2020-2022

Supervised by

Dr. Majid Ali

MASTER OF SCIENCE in

Thermal Energy Engineering

U.S-Pakistan Center for Advanced Studies in Energy (USPCAS-E)

National University of Sciences and Technology (NUST)

H-12, Islamabad 44000, Pakistan

August 2023

THESIS ACCEPTANCE CERTIFICATE

Certified that final copy of MS/MPhil thesis written by Muhammad Shummas Humayun (Registration No. 00000330307), of U.S.-Pakistan Centre for Advanced Studies in Energy has been vetted by undersigned, found complete in all respects as per NUST Statues/Regulations, is within the similarity indices limit and accepted as partial fulfillment for the award of MS/MPhil degree. It is further certified that necessary amendments as pointed out by GEC members of the scholar have also been incorporated in the said thesis.

Signature: _____
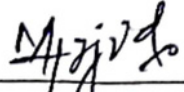
Name of Supervisor: Dr. Majid Ali

Date: _____16 Oct 2023_____

Signature (HoD): _____

Date: _____16 Oct 2023_____

Signature (Dean/Principal): _____
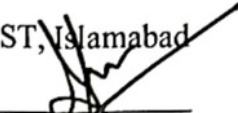
Date: _____

I

Certificate

This is to certify that work in this thesis has been carried out by **Mr. Muhammad Shummas Humayun** and completed under my supervision in, US-Pakistan Center for Advanced Studies in Energy (USPCAS-E), National University of Sciences and Technology, H-12, Islamabad, Pakistan.
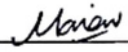
Supervisor:

_____
Dr. Majid Ali
USPCAS-E
NUST, Islamabad

GEC member 1:

_____
Dr. Adeel Waqas
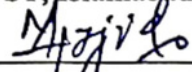USPCAS-E
NUST, Islamabad

GEC member 2:

_____
Dr. Mariam Mahmood
USPCAS-E
NUST, Islamabad

GEC member 3:

_____
Dr. Qazi Shahzad Ali
USPCAS-E
NUST, Islamabad

HOD-TEE:

_____
Dr Majid Ali
USPCAS-E
NUST, Islamabad

Dean/Principal:

_____
Dr Adeel Waqas
USPCAS-E
NUST, Islamabad

Dedication

To my dear parents, as well as my professors, who have always encouraged me to pursue my goals and motivated me to believe in myself; without their unwavering support, the completion of this project would not have been possible.

Abstract

Nuclear energy is considered as a zero-emission clean energy source. However, even though it can generate massive amounts of carbon-free electricity, potential accidents in nuclear power plants are a significant threat. Among these, the core meltdown is of significant concern. For environmental safety it is crucial to remove elemental radioactive iodine from flue gases through a system called FCVS (filtered containment venting system). Inside an FCVS, venturi scrubbers are significant, as they help remove the radioactive elements. Many studies have investigated the hydrodynamics of fluids inside venturi scrubbers and modelled the mass transfer of species between gases and scrubbing solutions. However, when it comes to modeling mass transfer coupled with a chemical reaction, the literature is very limited. Previous studies in literature have neglected the effect of chemical reaction on mass transfer. In this thesis, a UDF was developed to couple mass transfer of iodine and its reaction with Sodium Tetrathionate. The UDF was hooked to a commercial solver called Ansys Fluent, and CFD analysis was performed. The simulations were performed for three different gas flow rates and the resulting mass transfer enhancement was validated with experimental calculations present in the literature. The effect of droplet diameter on iodine removal efficiency was studied, and contours for mass fraction of iodine, thiosulfate, tetrathionate, and iodide along with hydrodynamics of the venturi scrubber were analyzed.

Keywords: Filtered Containment Venting System (FCVS), Iodine mass transfer, CFD, Venturi Scrubber, Iodine reaction

Table of Contents

List of Figures

List of Tables

List of Publications

1. Muhammad Shummas Humayun, Majid Ali, Muhammad Uzair Qureshi, Muhammad Bilal Khan Niazi, Yan Changqi, Sun Zongning, Gu Hai Feng, Yanmin Zhou, "CFD Analysis of Iodine Mass Transfer Coupled with a Chemical Reaction in a Filtered Containment Venting System," *Progress in Nuclear Energy*, 2023. (Submitted)

Chapter 1

Introduction

1.1. Background

The world's energy requirements are rapidly increasing due to industrialization and a growth in the population [1]. Due to this reason, the demands for fossil fuels have skyrocketed, resulting in increased Greenhouse gas emissions [2]. Based on estimations, the amount of CO2 release in the atmosphere can increase by approximately 64% in the year 2025 [3]. Due to this reason, use of sustainable and alternate energy sources needs to increase.

In this scenario, Nuclear Energy can be considered as a suitable alternative. Based on estimations, the electricity production from Nuclear Energy can increase by more than 200% by the year 2050 in the best case scenario, and conservative projection suggests an increase of at least of 16% from 2018 production levels (2563TWh) [4]. Unfortunately, accidents like reactor core meltdown are among the biggest risk factors of Nuclear power plants and require mitigation, as seen in Chernobyl, Fukushima Daichi, and the Three-Mile Island accidents [5].

For physical protection from radioactivity, the containment of a nuclear reactor generally comprises of multiple layers as shown in Figure 1.1, which if breached, can result in contamination of the environment with the radioactive materials [6].

The reactor containment vessel is the last barrier of defense against severe nuclear accidents to prevent releasing hazardous waste in the atmosphere. However, the containment vessel in the 2011 Fukushima Daichi accident failed to contain the pressure generated by the core's meltdown. This resulted in the release of radioactive material in lethal amounts into the atmosphere [7].

The potential emission of radioactive substances due to a mishap in a nuclear reactor can be broadly categorized into three distinct classifications. Initially, we have particulates, comprising of various substances disseminated in the form of aerosols or minuscule solid

particles. These may include volatile radionuclides represented in chemical formats such as hydroxides, oxides, and others alike. The ecological impact of these particulates is primarily contingent on the size of their constituent particles, as opposed to their inherent chemical makeup. Subsequently, we have Noble Gases that predominantly consist of xenon (Xe) and krypton (Kr) nuclides.

Noteworthy is the fact that due to their chemically unreactive nature, they do not undergo wet or dry deposition processes. As such, these gases do not get absorbed by human bodies upon inhalation. Their only potential detriment lies in the induction of cloud-shine. Iodine Nuclides are also deemed of substantial relevance. They are acknowledged to present themselves in three chemically distinct forms: particulate, as observed in cesium iodide; molecular or elemental iodine (I2); and organic iodide, exemplified by CH3I. [8].
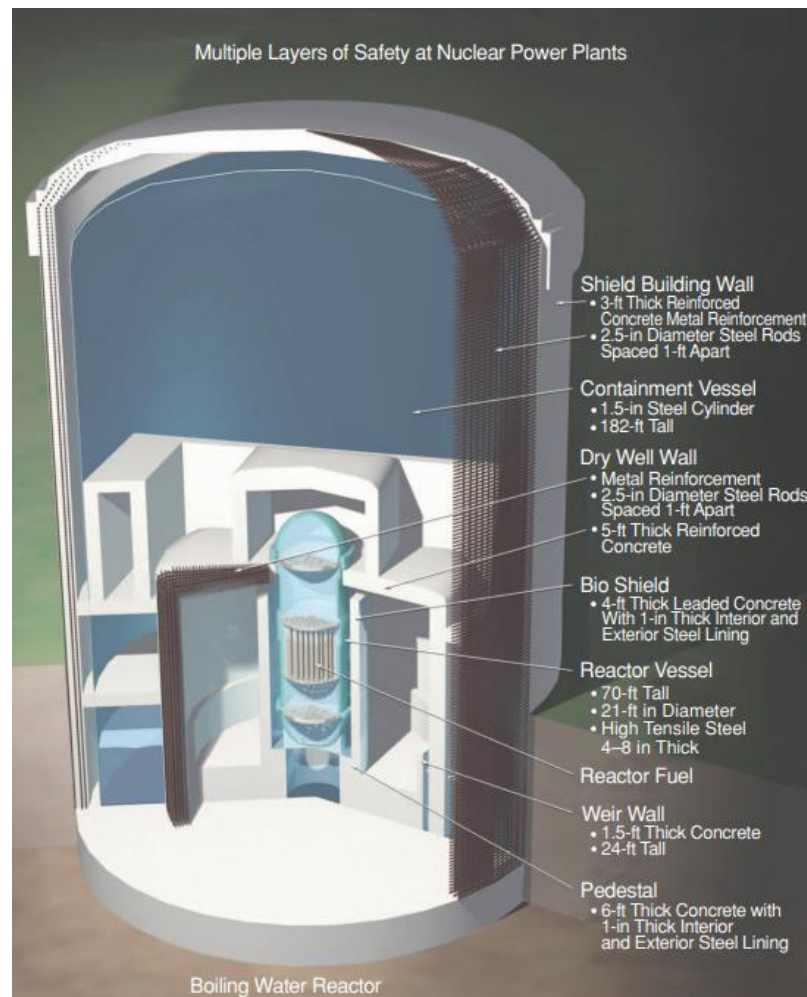
Fig. 1.1 Multiple safety layers of a boiling water nuclear reactor

Filtered containment venting systems (FCVS) are among the few safety systems that are designed to maintain the integrity of the containment in the case of steam buildup and core-meltdown. FCVS provides pressure relief inside the containment by venting out the air.

Venturi scrubbers are a common component of FCVS that remove radioactive and environmentally hazardous elements such as iodine-131 from the vented air to prevent contamination of the atmosphere. Such radioactive contaminants can increase the risks of thyroid cancer and other severe health conditions on exposure such as thyroid nodules, hypothyroidism, and autoimmune thyroiditis [9].

1.2. Filtered Containment Venting Systems

The Filtered Containment Venting System is comprised of a venturi scrubber, which is further succeeded by a metallic fiber filter, as depicted in Figure 1.2 [10]. The venturi scrubber encompasses three distinct sections: a convergent section, a throat, and a divergent section. The convergent section's function is to enhance the gas velocity by inducing a corresponding decrease in pressure. The throat, possessing uniform thickness, is typically the locus of the liquid-gas interaction. The divergent section allows for a partial recovery of the previously lost pressure in the convergent section and incites a decrease in gas velocity [11].
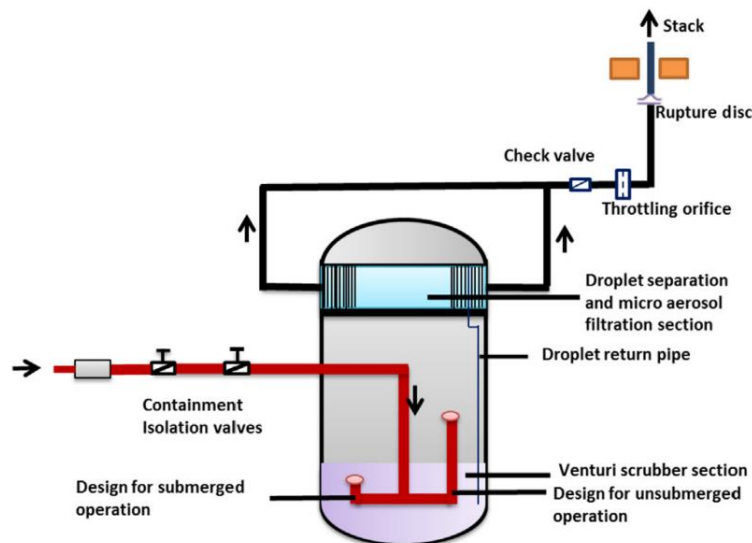
Fig. 1.2 Schematic diagram of a filtered containment venting system (FCVS)

The scrubber receives the liquid through two principal mechanisms, namely self-priming and forced feed. In the self-priming mechanism, the liquid is impelled into the venturi scrubber by exerting external pressure via pumps. Contrastingly, in the forced feed mechanism, the liquid is attracted into the venturi scrubber by the pressure differential established between the rapidly moving gas and the liquid's hydrostatic pressure [12].

This liquid is then introduced into the throat or the convergent section in the guise of spray droplets or a liquid film. An interaction between the liquid and gas phase transpires at the throat section, wherein the high-velocity gas triggers the droplet break-up of the liquid phase [13]. It is at this juncture where the interfacial mass transfer occurs between the gas phase and the scrubbing liquid.

Moreover, venturi scrubbers can be categorized into submerged and non-submerged types, the former requiring the gas at the divergent section's outlet to traverse through the liquid solution tank. Figure 1.3 provides a more detailed contrast between these two types.
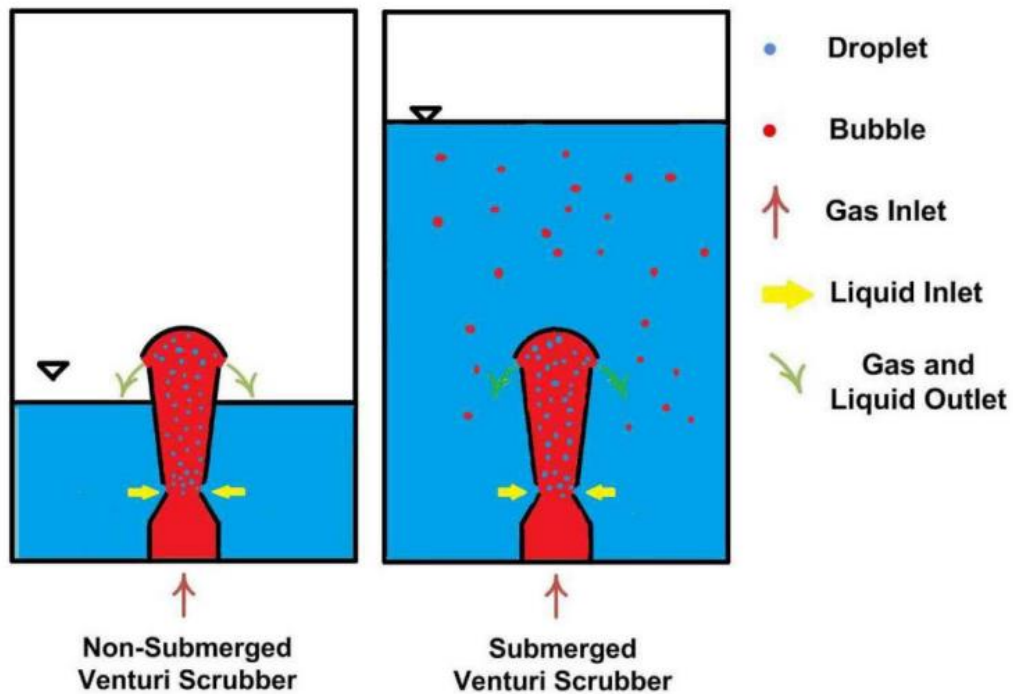
Fig. 1.3 Difference in submerged and non-submerged venturi scrubbers

Beyond the nuclear industry, venturi scrubbers are utilized extensively, spanning from controlling particulate matter emissions in industrial and commercial boilers fired with

coal, wood, liquid waste, and oil, to maintaining emissions from chemical process industries and municipal solid waste incinerators [14].

1.3. Interfacial Mass Transfer Accompanied with Chemical Reaction

The mass transferred within a single phase is contingent upon the concentration gradient of the transported species within that phase, a phenomenon termed diffusion. Nonetheless, mass may also transition from one phase to another, a process known as interfacial mass transfer. When the two phases come into contact, they are separated by an interface. Similar to single-phase mass transfer, interfacial mass transfer hinges on the concentration gradient of the transported species across both phases.

More precisely, interfacial mass transfer necessitates a departure from equilibrium, particularly at the interface. If a multiphase system is in equilibrium, no mass transfer occurs; however, when this equilibrium is disrupted, it will move toward re-establishing equilibrium.

Interfacial mass transfer is a critical phenomenon in industry, occurring in numerous engineering applications like distillation, separation and recovery operations, and chemical manufacturing processes. The efficacy of these processes can be enhanced by accelerating the rate of interfacial mass transfer, either by optimizing the system design, fine-tuning operating conditions, or via chemical reaction.

The early twentieth century marked the recognition of the potential of chemical reactions in enhancing mass transfer. It was observed that the chemical conversion of a solute occurring in the liquid phase could considerably expedite its transfer to the bulk liquid phase, thereby boosting the overall liquid mass transfer coefficient [15].

In the current study, the capture of iodine vapors is enhanced by their contact with a scrubbing solution of sodium thiosulfate, rather than mere water. The iodine rapidly reacts with sodium thiosulfate to undergo an irreversible chemical reaction, yielding sodium tetrathionate and sodium iodide, both of which are water-soluble. The chemical reaction can be written as [15]:

$$2Na_2S_2O_3 + I_2 \rightarrow 2NaI + Na_2S_4O_6 \tag{1}$$
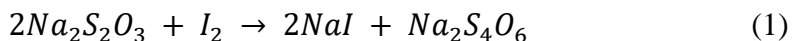
1.4. Computational Fluid Dynamics

Computational Fluid Dynamics (CFD) is a robust numerical tool employed to analyze processes and systems involving heat, mass, and momentum transfer. Over the years, CFD techniques have been applied extensively across industrial and non-industrial sectors for system analysis and design. Since the 1950s, CFD has been employed in the aerospace industry for designing and developing aircraft engines and bodies. The aerospace and automobile industries utilize CFD to compute drag force and airflow in the body [16].

In recent decades, CFD has been applied in the chemical and process sectors, such as in the simulation of combustion processes and multiphase flows in the system, and for the prediction of heat, mass, and momentum transfer [17]. Presently, CFD has become an integral component for the optimization and design of equipment and processes. Therefore, CFD has been used to predict the flows and performance of equipment in spray coating, heat exchanger, and other equipment. CFD serves as a numerical tool to anticipate the flow field, heat, and mass transfer rates. Additionally, phase changes (such as evaporation condensation), chemical reaction rates, and the mechanical movement of parts, such as turbines, can also be analyzed [18]. Recently, Computational Fluid Dynamics has been applied to understand the multifaceted flows and their thermophysical and rheological properties in multiphase flow mechanisms. Computational Fluid Dynamics resolves momentum, heat, and mass transfer by solving the governing equation on the control volume. The rate of change of the components is equivalent to the corresponding components applied force.

1.5. Research Objectives

To render nuclear energy more viable and safer, the installation of severe accident mitigation equipment is essential. In this context, CFD techniques are utilized to study various parameters and processes occurring in safety equipment.

The present work is concentrated on performing a CFD analysis to study the hydrodynamics and the mass transfer in the presence of a chemical reaction in a venturi scrubber for the absorption of iodine from vent gas by a scrubbing solution of sodium thiosulfate. The primary objectives of this research include:

- Develop a UDF for Iodine's mass transfer coupled with chemical reaction.

- To study the performance of iodine removal in venturi scrubber at different gas flow rates.
- To determine if liquid side film thickness can be safely neglected as it was done in previous studies related to this topic.
- Perform CFD contour analysis of various species involved in the mass transfer of iodine in the venturi scrubber.

1.6. Scope and Limitations

1.6.1. Scope

This study couples the mass transfer of iodine from gas to liquid phase in a venturi scrubber with its chemical reaction with Sodium Tetrathionate with the help of a user-defined function (UDF). The UDF incorporates the mathematical model of the chemical reaction, which is based on two-film theory and film-discretization. Previous studies in the literature have neglected the effect of the chemical reaction and only considered the gas-side mass transfer coefficient of iodine. The model is validated at different flow rates with past experimental data that is present in the literature, and flow contours of different species are analyzed.

1.6.2. Limitations

Some assumptions were made to model the chemical reaction of iodine in the liquid phase of the scrubber to reduce the complexity of the model. Firstly, it was assumed that all liquid droplets are spherical, with the same diameter, and a uniform distribution. Furthermore, the mathematical model has been based on the two-film theory, which assumes the formation of two mass transfer rate limiting films on either side of the interphase layer. The liquid side film thickness is assumed to be equal to the radius of the liquid droplets formed in the venturi scrubber. Due to these assumptions, the model overpredicts the iodine removal efficiency for low flow rates, but accurately validates for higher flow rates due to more uniform droplet distribution at high flow rates.

Summary

This chapter explores the escalating global energy needs and considers nuclear energy as a potential sustainable solution. It delves into the risks involved in nuclear energy production, focusing on the release of hazardous waste and the measures in place to contain it. Detailed discussion is provided on Filtered Containment Venting Systems (FCVS) and venturi scrubbers, devices designed to manage such risks. It explores interfacial mass transfer and its enhancement via chemical reactions, illustrated with the example of iodine capture by a scrubbing solution of sodium thiosulfate. It also necessitates the use of CFD as an analytical tool to understand these processes better.

References

[1]   P. Sadorsky, "The effect of urbanization and industrialization on energy use in emerging economies: Implications for sustainable development," *Am. J. Econ. Sociol.*, vol. 73, no. 2, pp. 392–409, 2014, doi: 10.1111/ajes.12072.

[2]   D. Hoornweg, L. Sugar, and C. L. T. Gómez, "Cities and greenhouse gas emissions: moving forward," *Environ. Urban.*, vol. 23, no. 1, pp. 207–227, 2011, doi: 10.1177/0956247810392270.

[3]   M. Akyol and E. Uçar, "Carbon footprint forecasting using time series data mining methods: the case of Turkey," *Environ. Sci. Pollut. Res.*, vol. 28, no. 29, pp. 38552–38562, 2021, doi: 10.1007/s11356-021-13431-6.

[4]   "Energy, electricity, and nuclear power estimates for the peri..|INIS." https://inis.iaea.org/search/search.aspx?orig_q=RN:35010284 (accessed May 30, 2022).

[5]   F. D'Auria, N. Debrecin, and H. Glaeser, "Strengthening nuclear reactor safety and analysis," *Nucl. Eng. Des.*, vol. 324, pp. 209–219, 2017, doi: https://doi.org/10.1016/j.nucengdes.2017.09.008.

[6]   J. D. MacDonald, "Safe and secure - Environmental effects of nuclear power plants and the nuclear fuel cycle," *IEEE Power Energy Mag.*, vol. 4, no. 6, pp. 49–55, 2006, doi: 10.1109/PAE-M.2006.247870.

[7]   I. Younus and M. S. Yim, "Out-containment mitigation of gaseous iodine by alkaline spray in severe accident situation," *Prog. Nucl. Energy*, vol. 83, pp. 167–176, 2015, doi: 10.1016/j.pnucene.2015.03.012.

[8]   I. T. Series, "Case Study on Assessment of Radiological Environmental Impact from Potential Exposure," *Iaea Tecdoc*, vol. 1914, p. 198, 2020, [Online]. Available: http://www-ns.iaea.org/standards/

[9]   E. Chirikova *et al.*, "Association between exposure to radioactive iodine after the Chernobyl accident and thyroid volume in Belarus 10-15 years later," *Environ. Heal.*, vol. 21, Jan. 2022, doi: 10.1186/s12940-021-00820-0.

[10] M. Bal, R. C. Jose, and B. C. Meikap, "Control of accidental discharge of radioactive materials by filtered containment venting system: A review," *Nucl. Eng. Technol.*, vol. 51, no. 4, pp. 931–942, 2019, doi: 10.1016/j.net.2019.01.008.

[11] J. A. S. Gonçalves, M. A. M. Costa, M. L. Aguiar, and J. R. Coury, "Atomization of liquids in a Pease-Anthony Venturi scrubber: Part II. Droplet dispersion," *J. Hazard. Mater.*, vol. 116, no. 1–2, pp. 147–157, 2004, doi: 10.1016/j.jhazmat.2004.08.030.

[12] M. Lehner, "Aerosol Separation Efficiency of a Venturi Scrubber Working in Self-Priming Mode," *Aerosol Sci. Technol.*, vol. 28, no. 5, pp. 389–402, 1998, doi: 10.1080/02786829808965533.

[13] M. Ali, Y. A. N. Chanqgi, S. U. N. Zhongning, G. U. Haifeng, W. Junlong, and K. Mehboob, "Iodine Removal Efficiency in Non-Submerged and submerged self-priming venturi scrubber," *Nucl. Eng. Technol.*, vol. 45, no. 2, pp. 203–210, 2013.

[14] C. Incinerator, "Air Pollution Control Technology Fact Sheet," pp. 1–6, 1998, [Online]. Available: https://www3.epa.gov/ttnchie1/mkb/documents/fcataly.pdf

[15] G. J. Evans and J. R. Ling, "Enhancement of the interfacial transfer of iodine by chemical reaction," *Can. J. Chem. Eng.*, vol. 78, no. 1, pp. 221–225, 2000, doi: 10.1002/cjce.5450780128.

[16] T. Sibilli and M. Savill, "Computational fluid dynamics drag prediction and decomposition for propulsive system integration," *Proc. ASME Turbo Expo*, vol. 1, no. January, pp. 257–264, 2011, doi: 10.1115/GT2011-46214.

[17] A. Rajora and J. W. Haverkort, "An analytical multiphase flow model for parallel plate electrolyzers," *Chem. Eng. Sci.*, vol. 260, p. 117823, 2022, doi: 10.1016/j.ces.2022.117823.

[18] S. Salehi, S. A. Madani, and R. Kiran, "Characterization of drilling fluids filtration through integrated laboratory experiments and CFD modeling," *J. Nat. Gas Sci. Eng.*, vol. 29, pp. 462–468, 2016, doi: 10.1016/j.jngse.2016.01.017.s

Chapter 2

Literature Review

Filtered containment venting systems (FCVS) are among the few safety systems that are designed to maintain the integrity of the containment in the case of steam buildup and core-meltdown. FCVS provides pressure relief inside the containment by venting out the air. Venturi scrubbers are a common component of FCVS that remove radioactive and environmentally hazardous elements such as iodine-131 from the vented air to prevent contamination of the atmosphere. Such radioactive contaminants can increase the risks of thyroid cancer and other severe health conditions on exposure such as thyroid nodules, hypothyroidism, and autoimmune thyroiditis [1].

A typical venturi scrubber geometry features a converging-diverging nozzle with the capability of handling a scrubbing solution. This scrubbing solution passes through the geometry and absorbs the contaminants present in the air. Leith et al. evaluated the pressure drop inside venturi scrubbers using a mathematical model [2]. It was found that pressure drop due to the variable cross-section and wall-friction losses is a critical parameter for determining a venturi scrubber's performance.

The liquid droplet size can have a direct impact on the mass transfer of gases inside a venturi scrubber. Alonso et al measured the water droplet diameters inside a venturi scrubber with a variation in the ratio between liquid and gas, and gas velocity [3]. This experimentation was validated with Sauter mean diameter calculated from equations given by Boll et al. [4]. It was found that gas velocity has a higher impact on the droplet size as compared to the ratio between liquid and gas flow.

Ananthanarayanan et.al. used ANSYS FLUENT to study the nozzle arrangement on flux distribution [5]. They found that uniform penetration multiple jet penetration gave 11-50% higher liquid owing to the effect of liquid rate and nozzle diameter. Ali et al. studied the hydrodynamics of venturi scrubber using the CFD Package ANSYS CFX. The k-ε turbulence model was used to compute the pressure drop [6]. The pressure drop was observed to increase with gas flow rate and the static pressure at water inlet.

Similarly, Gulhane et al. predicted the hydrodynamic behavior in the venturi scrubber using Eulerian-Eulerian approach in ANSYS Workbench [7]. The results showed that the pressure drop increased with mass flow rate of the gas phase. Manisha Bal et. al. studied the hydrodynamics of the venturi scrubber using the VOF model in ANSYS Fluent [8]. The pressure drop was observed to increase with the liquid mass flow rate, throat gas velocity and liquid to gas ratio.

Pak and Chang developed a numerical model to determine the collection efficiency and pressure drop inside a venturi scrubber for the removal of dust particles. Eulerian-Lagrangian approach was used for the numerical study involving a three-phase mixture of dust, air, and water [9].

Self-priming and force-feeding are the two most common types of venturi scrubbers. Ali et al. developed a mathematical model to determine the iodine removal efficiency of a self-priming venturi scrubber in both non-submerged and submerged cases. For the absorption of iodine, the aqueous scrubbing solution was composed of 0.2% sodium hydroxide and 0.5% sodium thiosulfate. The chemical reaction between iodine and the scrubbing solution was assumed to be rapid and hence, the gas side mass transfer coefficient was only used to calculate the mass transfer of iodine. The mathematical model was validated with experimentation. Results of the numerical model agreed with experiments for the case of submerged but under-predicted in the case of non-submerged venturi scrubbers [10]. Ashfaq et al. [11] used the numerical model developed by Ali et al. [10] to model the mass transfer of iodine in a venturi scrubber with a scrubbing solution of aqueous sodium hydroxide and water via a user-defined function in Ansys Fluent. It was observed that an increase in droplet diameter lowered the removal efficiency of iodine. Furthermore, they noted that closer to the throat the velocity achieved was higher for smaller droplet diameters.

Collection performance of aerosols in a self-priming venturi scrubber was studied by Zhou et al., with an experiment by varying parameters like gas velocity, nozzle dimensions, throat length, and diffuser angles. An increase in the aerosol retention efficiency was observed with an increase in injection flow rate and gas velocity. Furthermore, the aerosol retention performance was higher for long throat length and small diffuser angle [12].

Ahad et al., provided a modified mathematical model for the removal of Iodine in venturi scrubbers by adding new parameters such as bubble rise velocity, gas holdup, and jet penetration. Based on this mathematical model, a removal efficiency of 99.8% was achieved [13].

A theoretical model was proposed by Ravindram et al., to evaluate the removal efficiency of gaseous pollutants inside a venturi scrubber by incorporating an irreversible reaction between alkaline solutions and gases along with simultaneous diffusion. The model was validated with experimentation involving the removal of SO_2 and CO_2 using a scrubbing solution containing sodium hydroxide [14]. Hills et al. [15] developed a model for gas absorption in venturi scrubbers due to a chemical reaction. It was noted that the absorption of gases in a venturi scrubber is a diffusion-controlled rapid reaction.

Scheper et al. [16] provided a mechanism for the reaction between iodine and sodium thiosulfate which was in agreement with experimental results. Albert et al., developed a quasi-steady-state mass transfer mathematical model to determine the removal of iodine from a water spray. This model was used to study the changes in mass transfer rate due to the iodine hydrolysis reaction and a variance between 120.5% and 68.0% in the mathematical model was found in comparison with the experimental results [17].

Ling et al. researched on the enhancement effects of chemical reaction on the interfacial mass transfer of Iodine. She developed a model for simulations of such systems based on film discretization and this model was further validated with experimental study. A rate constant of 6.16 x 10^8 $M^{-1}s^{-1}$ for the reaction between sodium thiosulfate and iodine was reported after experimental calculations [18].

Goel et. al investigated the hydrodynamics and the iodine retention efficiency in a submerged venturi scrubber [19]. The simulation results were validated with experimental analysis. They found out that the increase in air flow rates upto a particular level as well as increase in submergence height caused an increase in iodine retention efficiency. However, they did not model the chemical reaction of iodine with the scrubbing solution and its effect on the overall mass transfer.

Safdar et. al modelled the scrubbing of sulfur dioxide in a venturi scrubber. Water was used as a scrubbing solution [20]. He included the chemical reaction of sulfur dioxide with

water in ANSYS Fluent and was able to predict the sulfurous acid concentration profile along the length of the venturi scrubber. It was found out that desulfurization efficiency increased with the gas mass flow rate, accession in L/G ratio and decrease in sulfur dioxide concentrations in the feed gas. His simulation, however, did not include the effect of chemical reaction in enhancement of mass transfer between gas and liquid phases.

Summary

When it comes to CFD analysis of iodine mass transfer in a venturi scrubber, studies in the literature have neglected the chemical reaction by considering it instantaneous. In other words, it was assumed that iodine will rapidly get consumed in the liquid phase, hence only the gas side mass transfer coefficient was considered. The hydrodynamics of venturi scrubbers has been studied extensively, and various studies have qualitatively and quantitatively validated the information present in the literature. However, the literature is very limited when it comes to modeling mass transfer in combination with chemical reactions in venturi scrubbers.

References

[1] E. Chirikova *et al.*, "Association between exposure to radioactive iodine after the Chernobyl accident and thyroid volume in Belarus 10-15 years later," *Environ. Heal.*, vol. 21, Jan. 2022.

[2] D. Leith, D. W. Cooper, and S. N. Rudnick, "Venturi Scrubbers: Pressure Loss and Regain," *Aerosol Sci. Technol.*, vol. 4, no. 2, pp. 239–243, Jan. 1985.

[3] D. Fernández Alonso, J. A. S. Gonçalves, B. J. Azzopardi, and J. R. Coury, "Drop size measurements in Venturi scrubbers," *Chem. Eng. Sci.*, vol. 56, no. 16, pp. 4901–4911, 2001.

[4] R. H. Boll, L. R. Fiais, P. W. Maurer, and W. L. Thompson, "Mean Drop Size in a Full Scale Venturi Scrubber via Transmissometer," *J. Air Pollut. Control Assoc.*, vol. 24, no. 10, pp. 934–938, 1974.

[5] N. V. Ananthanarayanan and S. Viswanathan, "Effect of nozzle arrangement on Venturi scrubber performance," *Ind. Eng. Chem. Res.*, vol. 38, no. 12, pp. 4889–4900, 1999.

[6] M. Ali, C. Yan, Z. Sun, J. Wang, and K. Mehboob, "CFD simulation of prediction of pressure drop in venturi scrubber," *Appl. Mech. Mater.*, vol. 166–169, pp. 3008–3011, 2012.

[7] N. P. Gulhane, H. S. Kadam, S. S. Kale, and M. T. Scholar, "Analysis of Pressure and Velocity at the Throat of Self-Priming Venturi Scrubber," *J. Mater. Sci. Mech. Eng.*, vol. 2, no. 6, pp. 57–61, 2015.

[8] M. Bal and B. C. Meikap, "Prediction of hydrodynamic characteristics of a venturi scrubber by using CFD simulation," *South African J. Chem. Eng.*, vol. 24, pp. 222–231, 2017.

[9] S. I. Pak and K. S. Chang, "Performance estimation of a Venturi scrubber using a computational model for capturing dust particles with liquid spray," *J. Hazard. Mater.*, vol. 138, no. 3, pp. 560–573, 2006.

[10] M. Ali, Y. A. N. Chanqgi, S. U. N. Zhongning, G. U. Haifeng, W. Junlong, and K.

Mehboob, "Iodine Removal Efficiency in Non-Submerged and submerged self-priming venturi scrubber," *Nucl. Eng. Technol.*, vol. 45, no. 2, pp. 203–210, 2013.

[11]   T. Ashfaq *et al.*, "CFD investigation of iodine mass transfer in venturi scrubbing solution of Filtered Containment Venting System," *Prog. Nucl. Energy*, vol. 111, pp. 195–204, Mar. 2019.

[12]   Y. Zhou, Z. Sun, H. Gu, and Z. Miao, "Experimental research on aerosols collection performance of self-priming venturi scrubber in FCVS," *Prog. Nucl. Energy*, vol. 85, pp. 771–777, 2015.

[13]   J. Ahad *et al.*, "Study of hydrodynamics and iodine removal by self-priming venturi scrubber," *Nucl. Eng. Technol.*, vol. 55, no. 1, pp. 169–179, 2023.

[14]   M. Ravindram and P. Naidu, "Modeling of a venturi scrubber for the control of gaseous pollutants," *Ind. Eng. Chem. Process Des. Dev.*, vol. 25, no. 1, pp. 35–40, Jan. 1986.

[15]   J. H. Hills, "Behavior of Venturi Scrubbers as Chemical Reactors," *Ind. Eng. Chem. Res.*, vol. 34, no. 12, pp. 4254–4259, Dec. 1995.

[16]   W. M. Scheper and D. W. Margerum, "Non-Metal Redox Kinetics Reactions of Iodine and Triiodide with Thiosulfate via 12Sz032- and IS203- Intermediates," no. 7, pp. 5466–5473, 1992.

[17]   M. F. Albert, J. S. Watson, and R. P. Wichner, "The Absorption of Gaseous Iodine by Water Droplets," *Nucl. Technol.*, vol. 77, no. 2, pp. 161–174, May 1987.

[18]   G. J. Evans and J. R. Ling, "Enhancement of the interfacial transfer of iodine by chemical reaction," *Can. J. Chem. Eng.*, vol. 78, no. 1, pp. 221–225, 2000.

[19]   P. Goel, A. Moharana, and A. K. Nayak, "Numerical simulation of injection characteristics, hydrodynamics and absorption of iodine vapour in a venturi scrubber operating in self-priming mode," *Nucl. Eng. Des.*, vol. 341, pp. 360–367, 2019.

[20]   I. Safdar, M. Zubair, N. Iqbal, and M. Ali, "CFD simulation of chemical reaction between sulfur dioxide and water in a venturi scrubber," *Sep. Sci. Technol.*, vol. 55.

Chapter 3

Methodology

The applications of venturi scrubber range in a variety of industries like petroleum, nuclear, chemical processing etc. where vent gas is to be cleaned efficiently at a lower operating cost. As mentioned in the previous chapter CFD has been exploited to study the flow and mass transfer in a venturi scrubber. However, to the author's best of knowledge CFD has not yet been applied to study the enhancement occurring in mass transfer due to a chemical reaction in gas liquid absorption systems.

3.1. CFD Methodology

To analyze the problem in CFD, the scientific knowledge is to interoperate mathematically by adding the required information in software, the software expresses the stated problem in scientific term. The CFD solves the problem in three major parts.

- Pre-processing
- Solving
- Post-processing

3.1.1. Pre-Processing

Pre-processing in Computational Fluid Dynamics (CFD) using Ansys Fluent involves several crucial steps that prepare the problem for numerical computation.

The physical problem's domain is represented as a 3D object. This is geometry. Fluent allows importing geometry from various CAD programs, or users can create simple geometries within the program. In this study, geometry was made using Solidworks and imported into Ansys ICEM CFD module for preprocessing.

The next step is to discretize the geometry into a finite number of control volumes (cells or elements) in a process called meshing. The quality of the mesh significantly impacts the accuracy and stability of the simulation. Fluent includes tools to refine the mesh, ensuring it is well-resolved in areas with high gradients.

It is also crucial to define boundary conditions at all domain boundaries. In Fluent, boundary conditions can represent inlet and outlet flows, walls, symmetry planes, periodic boundaries, and more. Correctly specifying boundary conditions is crucial for the accuracy and convergence of the simulation.

Depending on the problem, users may need to include models for turbulence, heat transfer, multiphase flow, chemical reactions, and more. Fluent provides a variety of built-in models for these phenomena.

The physical properties of the materials (fluids, solids) involved in the simulation are defined. This includes properties like density, viscosity, and specific heat capacity. Fluent includes databases of properties for many common materials.

3.1.2. Solving

The solving phase is where the actual numerical computation takes place. Fluent offers several options for the numerical scheme to be used in the solver, which can be adjusted based on the problem's requirements. There are also settings related to the handling of pressure-velocity coupling (algorithms like SIMPLE, PISO), discretization schemes (upwind, central differencing, etc.), and solution controls.

Fluent allows users to initialize the flow field with estimates of the flow variables (velocity, pressure, temperature, etc.). A good initialization can accelerate the convergence of the solution.

The solver iteratively solves the governing equations until convergence criteria are met. Fluent provides real-time monitors to check residuals, which measure the imbalances in the solved equations. Residuals decreasing to a low level generally indicate convergence.

Following are the different techniques to solve the CFD:
- Finite Difference Method
- Finite Element Method
- Finite Volume Method

When the grid generation is generated the computational Fluid Dynamic problem can be initialized. The generated mesh is exported to solve program where the CFD analysis must be done. The CFD solver requires the initial boundary conditions values which must be

given in pre-processing. The algorithm of the finite volume method is used in ANSYS Fluent and consists of the following steps:

- The governing equation is solved by integration of flow field, heat and mass transfer equation in computational domain.
- Discretization, of governing equation which converts the integral equation into algebraic equation using Finite Difference approach.
- The algebraic equation is solved by iteration either in steady state or in transient state.

3.1.3. Post-processing

Post-processing is the final stage in the CFD process, where the computed results are analyzed and visualized.

Fluent provides comprehensive tools for visualizing the simulation results, including contour plots, vector plots, pathlines/streamlines, and animations. These can be used to visualize the distribution and behavior of flow variables like velocity, pressure, temperature, turbulence, etc.

This step involves extracting numerical data at points, lines, or surfaces in the domain for further analysis. Fluent can export this data for use in other software. It allows interpreting the results and drawing conclusions about the original physical problem. It's also crucial to validate the results, comparing them with experimental data or known solutions whenever possible to ensure the CFD simulation accurately represents reality.

3.2. Simulation Methodology Flow Chart

Creation of 3-D Geometry in ICEM CFD

↓

Generating 3-D Mesh in ICEM CFD

↓

Importing Mesh in ANSYS FLUENT

↓

Creating Define Adjust UDF for Mass Transfer coupled with Chemical Reaction

↓

Creating Define Mass Transfer UDF for Mass Transfer

↓

Creating Define VR Rate UDF for Chemical Reaction

↓

Compiling and Hooking UDFs in ANSYS FLUENT

↓

Setting up Solver in FLUENT

↓

Running Solution

↓

Post Processing the results in CFD Post

3.3. Eulerian-Eulerian Two Fluid Model

CFD has emerged as a valuable method to examine multi-phase flows. These flows could be studied by either the Eulerian-Lagrangian or the Eulerian-Eulerian approach. In the former, the continuous phase is modeled using the Eulerian frame of reference, tracking changes in phase properties within static cells and calculating accordingly, while the dispersed phase is modeled using the Lagrangian frame of reference, tracking each particle of the dispersed phase. Although this method enhances result accuracy, it requires substantial computational resources, making it infeasible for complex applications. Conversely, the Eulerian-Eulerian approach models both continuous and dispersed phases in the Eulerian frame of reference, offering satisfactory results with a relatively lower requirement of computational resources.

In this study ANSYS Fluent with Eulerian-Eulerian approach was used to simulate the multi-phase flow of air-iodine mixture and scrubbing solution of sodium thiosulfate. The parameters like pressure, velocity and volume fraction were analyzed to study the hydrodynamics of the system.

The Eulerian-Eulerian approach views the two phases as interpenetrating continua, such that the volume of one phase does not overlap with the volume occupied by the other phase. The sum of the volume fraction of all phases equals unity, as illustrated by the equation:

$$\sum_{q=0}^{n} \alpha_q = 1 \tag{1}$$

The volume fraction of each phase is represented by α_q and n represents the total number of phases. In this study, two phases are present (1) Primary gas phase comprising of air-iodine mixture (iodine mass fraction of 0.2) and (2) Secondary liquid phase comprising of scrubbing solution of sodium thiosulfate (5 wt %) which are represented by 'a' and 's' respectively.

3.3.1. Continuity Equation

The EE approach solves a set of n continuity and momentum equation which are given as follows [1]. The continuity equation for gas 'g' and liquid 'l' phase are:

$$\frac{\partial}{\partial t}(\alpha_g \rho_g) + \nabla.(\alpha_g \rho_g v_g) = 0 \tag{2}$$

$$\frac{\partial}{\partial t}(\alpha_l \rho_l) + \nabla.(\alpha_l \rho_l v_l) = 0 \tag{3}$$

3.3.2. Conservation of Momentum

The momentum conservation term for the gas phase is:

$$\frac{\partial}{\partial t}(\alpha_g \rho_g \vec{v_g}) + \nabla.(\alpha_g \rho_g \vec{v_g}\vec{v_g}) = -\alpha_g \nabla p + \nabla.\bar{\bar{\tau}}_g + \varepsilon_g \rho_g \vec{g} - K_{gl}(\vec{v_g} - \vec{v_l}) \tag{4}$$

The gas phase stress–strain tensor and is given by:

$$\bar{\bar{\tau}}_g = \alpha_g \mu_g \left(\nabla \vec{v_g} + \nabla \vec{v_g^T}\right) + \varepsilon_g \left(\lambda_g - \frac{2}{3}*\mu_g\right).\nabla \vec{v_g}\bar{I} \tag{5}$$

The momentum exchange term for the liquid phase is written as:

$$\frac{\partial}{\partial t}(\alpha_l \rho_l \vec{v_l}) + \nabla.(\alpha_l \rho_l \vec{v_l}\vec{v_l}) = -\alpha_l \nabla p - \nabla p_l + \nabla \bar{\bar{\tau}}_l + \alpha_l \rho_l \vec{g} - K_{gl}(\vec{v_g} - \vec{v_l}) \tag{6}$$

Liquid phase stress tensors are given by:

$$\bar{\bar{\tau}}_l = \alpha_g \mu_l \left(\nabla \vec{v_l} + \nabla \vec{v_l^T}\right) + \varepsilon_l \left(\lambda_l - \frac{2}{3}*\mu_l\right).\nabla \vec{v_l}\bar{I} \tag{7}$$

$$\mu_l = \frac{\alpha_l d_l \rho_l \sqrt{\theta_l \pi}}{6(3-e_{ll})}[1 + \frac{2}{5}(1+e_{ll})(3e_{ll}-1)\alpha_l g_{0,ll} \tag{8}$$

23

3.4. Turbulence Model in CFD

The two-equation models are the most used turbulence models in CFD particularly for industrial purposes. Two transport equations are solved by these models. The Reynolds Stresses are modeled using Eddy Viscosity. The standard k-ε model lies in this category. The robustness of calculation, reasonable accuracy and computationally less expensive have become a reason for its widespread use in the industrial flow and heat transfer simulations [2].

In this study the turbulence has been modeled using RNG k-ε turbulence model. The statistical technique of renormalization group theory (RNG) is applied to the Navier-Stokes equation to derive this model. The added advantages of using RNG model over standard k-ε model are:

- Performs more precisely for swirling and rapidly strained flows.
- The turbulent Prandtl numbers are calculated analytically as compared to user-specified constant values for standard k-ε model.
- Includes the low-Reynolds number effects.

3.4.1. Transport Equations for the RNG k-ε Model

This study uses the RNG k-ε turbulence model. The RNG k-ε turbulence model is derived from the Navier-Stokes equation by applying the RNG (renormalization group theory). It is widely used in heat transfer and industrial flow simulations due to its reasonably high accuracy while keeping the computational costs minimal. The transport equations for RNG k-ε model are as follows:

$$\frac{\partial}{\partial t}(\rho k) + \frac{\partial}{\partial x_i}(\rho k u_i) = \frac{\partial}{\partial x_j}\left(\alpha_k \mu_{eff} \frac{\partial k}{\partial x_j}\right) + G_k + G_b - \rho\varepsilon - Y_M + S_k \qquad (9)$$

$$\frac{\partial}{\partial t}(\rho\varepsilon) + \frac{\partial}{\partial x_i}(\rho\varepsilon u_i) = \frac{\partial}{\partial x_j}\left(\alpha_\varepsilon \mu_{eff} \frac{\partial \varepsilon}{\partial x_j}\right) + C_{1\varepsilon}\frac{\varepsilon}{k}(G_k + C_{3\varepsilon}G_b) - C_{2\varepsilon}\rho\frac{\varepsilon^2}{k} - R_\varepsilon + S_\varepsilon \qquad (10)$$

24

3.5. Mass Transfer Equations

Some basic principles pertaining to chemical engineering are presented in this section which are used in this study.

3.5.1. Diffusion Equation

The diffusion of particles in spherical coordinates in an unsteady state is given by Fick's second law as follows [3]:

$$\frac{\partial C}{\partial t} = Dab \left(\frac{2}{r} \frac{\partial C}{\partial r} + \frac{\partial^2 C}{\partial r^2} \right) \tag{11}$$

3.5.2. Interfacial Mass Transfer

The two-film theory approach is used to describe the interphase mass of iodine from gas to liquid phase. The two-film theory approach explains that, laminar layer exists at each interphase of the fluid turbulence is negligible at the interface

The turbulent eddies supplement action provides resistance to mass transfer progressively smaller. The concentration gradient for equimolar counter diffusion is almost linear close to the interphase.

The two-film theory is based on two hypothetical layers on either side of interphase in which the mass transfer takes place due to molecular diffusion. In this zone there is linear concentration gradient and outside the zone there is no concentration gradient [4].
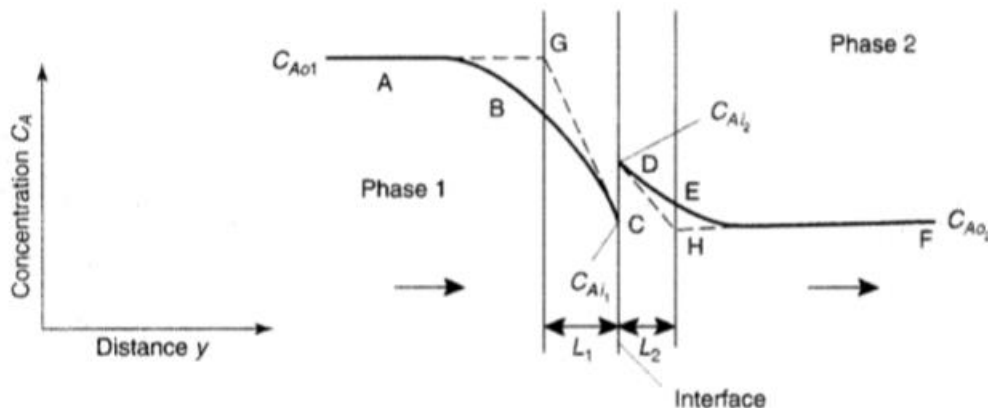

Fig. 3.1 Schematic of two film theory

For equimolar counter diffusion the mass transfer rate per unit area for the gas phase film is represented in the equations:

$$N_A = \frac{D_g}{\delta_g}(C_{Aog} - C_{Aig}) = k_g(C_{Aog} - C_{Aig}) \tag{12}$$

$$N_A = \frac{D_l}{\delta_l}(C_{Ail} - C_{Aol}) = k_l(C_{Ail} - C_{Aol}) \tag{13}$$

$$\frac{k_g}{k_l} = \frac{C_{Ail}}{C_{Aog}} - \frac{C_{Aol}}{C_{Aig}} \tag{14}$$

The phase equilibrium relationship given in equation 3.14 is used to determine the concentration of species between the interphases. The mass transfer coefficient is inversely proportional to the ratio of concentration of species. According to the relation the interphase coefficient will be adjusted, if the relative values of coefficients change the concentration will change too. The effective film thickness will be reduced by increasing the turbulence which result in increase of mass transfer coefficient [4].

3.5.3. Mass Transfer Coefficients

Without bulk flow the rate of mass transfer is proportional to the concentration gradient which is the driving force [4].

$$N_A = k(C_{Ai} - C_{Ao}) \tag{15}$$

Here, 'k' is directly proportional to the diffusivity and inverse relationship with the film thickness.

The two-film theory assumes a steady state process, so interface composition remains constant with respect to time. Since there is no accumulation in both the films the mass transfer rate will be the same for both phases [5].

$$N_A k_g(C_{Ao1} - C_{Ai1}) = k_l(C_{Ai2} - C_{Ao2}) \tag{16}$$

When there is phase equilibrium relationship there is no resistance to mass transfer for the general case and the mass transfer is considered for overall process.

$$N_A = K_{og}(C_{Aog} - C_{Aeg}) = K_{ol}(C_{Ael} - C_{Aol}) \tag{17}$$

The C_{Aog} and C_{Aol} are the concentrations of gas and liquid phases in the bulk phase and C_{Ae1} and C_{Ae2} are the concentrations of gas and liquid phases at equilibrium. If the equilibrium relationship is linear:

$$\frac{C_{Aig}}{C_{Ail}} = \frac{C_{Aeg}}{C_{Aol}} = \frac{C_{Aog}}{C_{Ael}} \tag{18}$$

The liquid and gas mass transfer coefficients can be related by the following equations:

$$\frac{1}{k_g} = \frac{1}{k_l}\frac{C_{Aig} - C_{Aog}}{C_{Aol} - C_{Ail}} \tag{19}$$

$$\frac{1}{K_{og}} = \frac{1}{k_g} + \frac{1}{k_l}\left(\frac{C_{Aeg} - C_{Aig}}{C_{Aig} - C_{Aog}}\right)\left(\frac{C_{Aig} - C_{Aog}}{C_{Aol} - C_{Ail}}\right) \tag{20}$$

$$\frac{1}{K_{og}} = \frac{1}{k_g}\frac{C_{Aeg} - C_{Aog}}{C_{Aig} - C_{Aog}} = \frac{1}{k_g}\frac{C_{Aeg} - C_{Aig}}{C_{Aig} - C_{Aog}} + \frac{1}{k_g}\frac{C_{Aig} - C_{Aog}}{C_{Aig} - C_{Aog}} \tag{21}$$

$$\frac{1}{K_{og}} = \frac{1}{k_g}\frac{C_{Aeg} - C_{Aog}}{C_{Aig} - C_{Aog}} = \frac{1}{k_g}\frac{C_{Aeg} - C_{Aig}}{C_{Aig} - C_{Aog}} + \frac{1}{k_g}\frac{C_{Aig} - C_{Aog}}{C_{Aig} - C_{Aog}} \tag{22}$$

$$\frac{C_{Aeg} - C_{Aig}}{C_{Aol} - C_{Ail}} = H \tag{23}$$

$$\frac{1}{K_{og}} = \frac{1}{k_g} + \frac{H}{k_l} \tag{24}$$

$$\frac{1}{K_{ol}} = \frac{1}{Hk_g} + \frac{1}{k_l} \tag{25}$$

$$\frac{1}{K_{og}} = \frac{H}{K_{ol}} \tag{26}$$

It can be seen, that when k_g is large compared to k_l, K_{ol} and k_g are approximately equal and when k_l is large compared with k_g, K_{og} and k_l are almost equal. The mass transfer rate is in linear relation with the driving force, so a straight-line graph is made at equilibrium.

3.5.4. Mass Transfer with Chemical Reaction

In the liquid phase as the iodine diffuses into the liquid film it is simultaneously being consumed by the second order irreversible chemical reaction with sodium thiosulfate. Detailed mechanism of chemical reaction has been proposed by Scheper et. al. is mentioned in Table 3.1 [6].

Table 3.1 Reaction rate constants

Reaction	k_f (Forward Rate Constant)	k_b (Backward Rate Constant)
$I_2 + I^- \leftrightarrow I_3^-$	5.6×10^9 M^{-1}s^{-1}	7.5×10^6 s^{-1}
$I_2 + S_2O_3^{2-} \leftrightarrow$ $I_2S_2O_3^{2-}$	7.8×10^9 M^{-1}s^{-1}	2.5×10^2 s^{-1}
$I_3^- + S_2O_3^{2-} \leftrightarrow$ $I_2S_2O_3^{2-} + I^-$	4.2×10^8 M^{-1}s^{-1}	9.5×10^3 M^{-1}s^{-1}
$I_2S_2O_3^{2-} \leftrightarrow IS_2O_3^{2-} +$ I^-	$0.245 \times k_b$	$0.245/k_f$
$IS_2O_3^{2-} + S_2O_3^{2-} \rightarrow I^-$ $+ S_4O_6^{2-}$	1.29×10^6 M^{-1}s^{-1}	-

As iodine diffuses out of the gas phase into the liquid phase, it is consumed simultaneously in a 2nd order irreversible chemical reaction with sodium thiosulfate. The mass balance coupled with chemical reaction and diffusion is given as:

$$\frac{\partial C}{\partial t} = D_l \frac{\partial^2 C}{\partial x^2} - r_i(x,t) \tag{27}$$

On the other hand, Fick's second law notes the diffusion of particles in spherical coordinates of an unsteady state system by the following equation [7]:

$$\frac{\partial C}{\partial t} = Dab \left(\frac{2}{r} \frac{\partial C}{\partial r} + \frac{\partial^2 C}{\partial r^2} \right) \tag{28}$$

Combining both equations, we arrive at the following equation for the overall mass balance:

$$\frac{\partial C}{\partial t} = D_l \left(\frac{2}{r} \frac{\partial C}{\partial r} + \frac{\partial^2 C}{\partial r^2} \right) - r_i(x, t) \tag{29}$$

Streinberger and Treybal correlation were used for the calculation of the gas side mass transfer coefficient for a single liquid phase droplet [8]. The diffusion coefficient of iodine was taken from correlations by Knudsenn et al., which is calculated as 8.97 x 10^{-6} m^2/s [9].

Since the consumption of is iodine assumed to be limited to the liquid film side only, the liquid side mass transfer coefficient depends on the rate of reaction of iodine with thiosulfate ions. It was assumed that all liquid droplets are spherical and have the same diameter with uniform distribution.
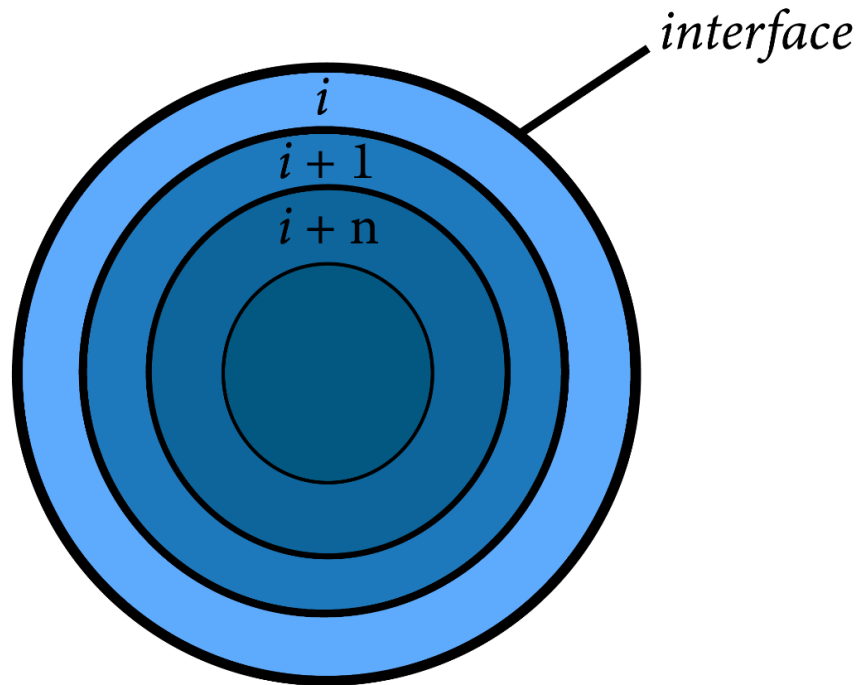

Fig. 3.2 Discretized elements of liquid film

A theoretical model developed by Ling et al. is used according to which we discretize the liquid film in seven elements of uniform thickness as shown in Figure 3.2 [10].

The following equation is used to calculate the diffusion in each discretized film:

$$\frac{\partial C_i}{\partial t} = D_l \left(\frac{2}{r} \left(\frac{c_{i+1} - c_i}{s} \right) + \left(\frac{c_{i-1} - 2c_i + c_{i+1}}{s^2} \right) \right) \tag{30}$$

Where $'s'$ refers to the thickness of each discretized element of film and is given as:

$$s = \frac{\delta_l}{7} \tag{31}$$

Based on this, the overall mass balance on every discretized element of film thickness is given as:

$$\frac{\partial C_i}{\partial t} = D_l \left(\frac{2}{r} \left(\frac{c_{i+1} - c_i}{s} \right) + \left(\frac{c_{i-1} - 2c_i + c_{i+1}}{s^2} \right) \right) - r_i(x, t) \tag{32}$$

Here, $r_i(x, t)$ is the rate of the reaction between sodium thiosulfate and iodine, and it is given as:

$$r_i = k_r C_i C_t \tag{33}$$

In the above equation, k_r is the reaction rate constant, taken as 6.16×10^8 M^{-1}s^{-1} based on experimental calculations by Ling et al. while C_t and C_i refer to the concentration of thiosulfate and iodine in the liquid phase [10].

The higher the rate of reaction, the lesser the concentration of iodine in the discretized element. As the reaction rate increases, the concentration of iodine subsequently approaches zero which reduces the liquid side film thickness. The new film thickness value is used for the evaluation of 's'. We assume that the droplet film thickness is equal to the droplet's radius, as validated by the experiments performed by Roseanne et. al. [10].

The partition coefficient *(H)* is taken as 74 based on calculations by Sander et al. [11]. After calculating the gas side and liquid side mass transfer coefficient, the overall mass transfer coefficient can be calculated.

Then the overall removal efficiency of iodine in the scrubber is calculated using the following equation:

$$\text{Removal Efficiency} = \frac{(X_i - X_o)}{X_i} \times 100 \tag{34}$$

Summary

This chapter covers the CFD methodology used in this thesis in detail. It starts by briefly describing the processes in a CFD setup followed by an explanation of the Eulerian-Eulerian approach used in this study. Furthermore, the turbulence model has also been detailed, with the transport equations that are being used by the solver. Finally, the mathematical model of mass transfer of iodine has been presented. This mass transfer is based on the two-film theory, and it has been coupled with the chemical reaction of iodine based on film discretization.

References

[1] ANSYS Fluent 12.0, "Fluent12," *ANSYS FLUENT 12.0 User's Guid.*, no. April, pp. 1–2070, 2009.

[2] B. E. Launder and D. B. Spalding, "The numerical computation of turbulent flows," *Comput. Methods Appl. Mech. Eng.*, vol. 3, no. 2, pp. 269–289, 1974.

[3] P. Goel, A. Moharana, and A. K. Nayak, "Numerical simulation of injection characteristics, hydrodynamics and absorption of iodine vapour in a venturi scrubber operating in self-priming mode," *Nucl. Eng. Des.*, vol. 341, pp. 360–367, 2019.

[4] R. Chhabra and V. Shankar, *Coulson and Richardson's chemical engineering: Seventh edition*. 2017.

[5] P. M. Doran, *Engineering Principles Second Edition*. 2013.

[6] W. M. Scheper and D. W. Margerum, "Non-Metal Redox Kinetics Reactions of Iodine and Triiodide with Thiosulfate via 12Sz032- and IS203- Intermediates," no. 7, pp. 5466–5473, 1992.

[7] D. J. Nicolin, D. F. Rossoni, and L. M. M. Jorge, "Study of uncertainty in the fitting of diffusivity of Fick's Second Law of Diffusion with the use of Bootstrap Method," *J. Food Eng.*, vol. 184, pp. 63–68, 2016.

[8] R. L. Steinberger and R. E. Treybal, "Mass transfer from a solid soluble sphere to a flowing liquid stream," *AIChE J.*, vol. 6, no. 2, pp. 227–232, 1960.

[9] J. G. Knudsen, "Properties of Air-Steam Mixtures Containing Small Amounts of Iodine.".

[10] G. J. Evans and J. R. Ling, "Enhancement of the interfacial transfer of iodine by chemical reaction," *Can. J. Chem. Eng.*, vol. 78, no. 1, pp. 221–225, 2000.

[11] R. Sander, "Compilation of Henry' s Law Constants for Inorganic and Organic Species of Potential Importance in Environmental Chemistry," *Database*, vol. 1, no. 1, pp. 1–107, 1999.

Chapter 4

CFD Simulation Setup

4.1. Geometry and Meshing

Geometry consists of a liquid inlet, a gas inlet, and a mixture outlet. The liquid enters the geometry along the sides and then converges towards the throat due to a Bernoulli effect. Both the liquid and gas meet at the throat opening where the mass transfer and reaction takes place.
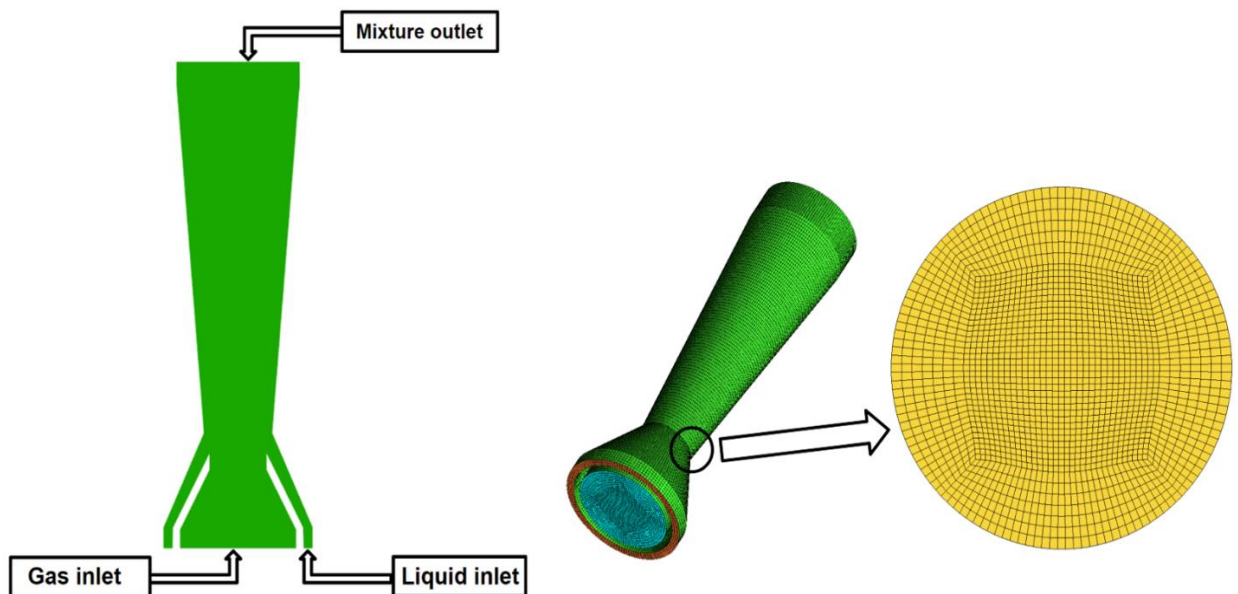

Fig. 4.1 Geometry and mesh of venturi scrubber

The geometry was first created in Solidworks and then transported into ICEM CFD meshing module. First, the geometry was blocked, and parts were named. The blocks were split into multiple sections, to divide the geometry and make the meshing process easier.

The geometry was split into a quarter section due to its symmetrical nature. To account for the rounded sections of the venturi scrubber, two o-grids were generated, and parts of the blocks were deleted to account for the empty space between the liquid inlet and the gas inlet.
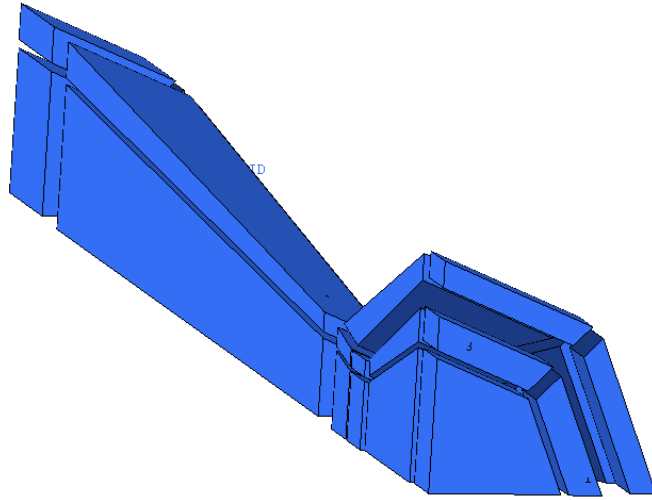
Fig. 4.2 Blocking of 1 quarter of the geometry

The blocks were then associated with the parts of the geometry and node lengths were set as shown in figure 4.2, followed by the generation of a premesh. A structured HEXA mesh was created with a total of 110426 elements and 101532 total nodes.

Fig. 4.3 Pre-mesh of 1 quarter of the geometry

35

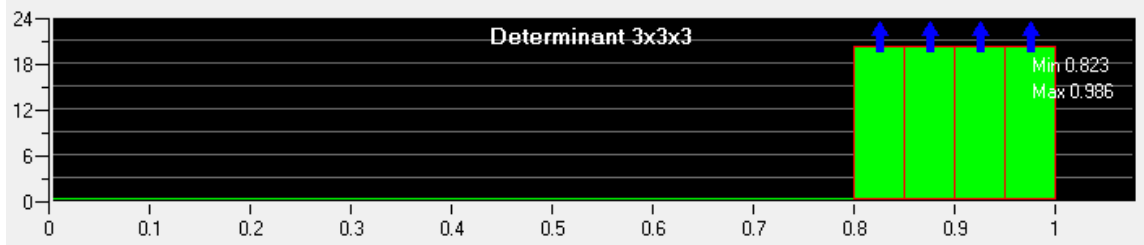A minimum quality of 0.0.823 was achieved with Determinant 3x3x3 as the meshing quality criteria as shown in figure 4.4:

Fig. 4.4 Determinant 3x3x3 quality criteria

The number of mesh elements were selected after performing a mesh independence study by varying the number of elements in the mesh and observing the results. At around 110,000 elements, the graph of the independence test turns out to be rather constant which suggests that the resulting factors are no longer dependent on the sensitivity of the grid.
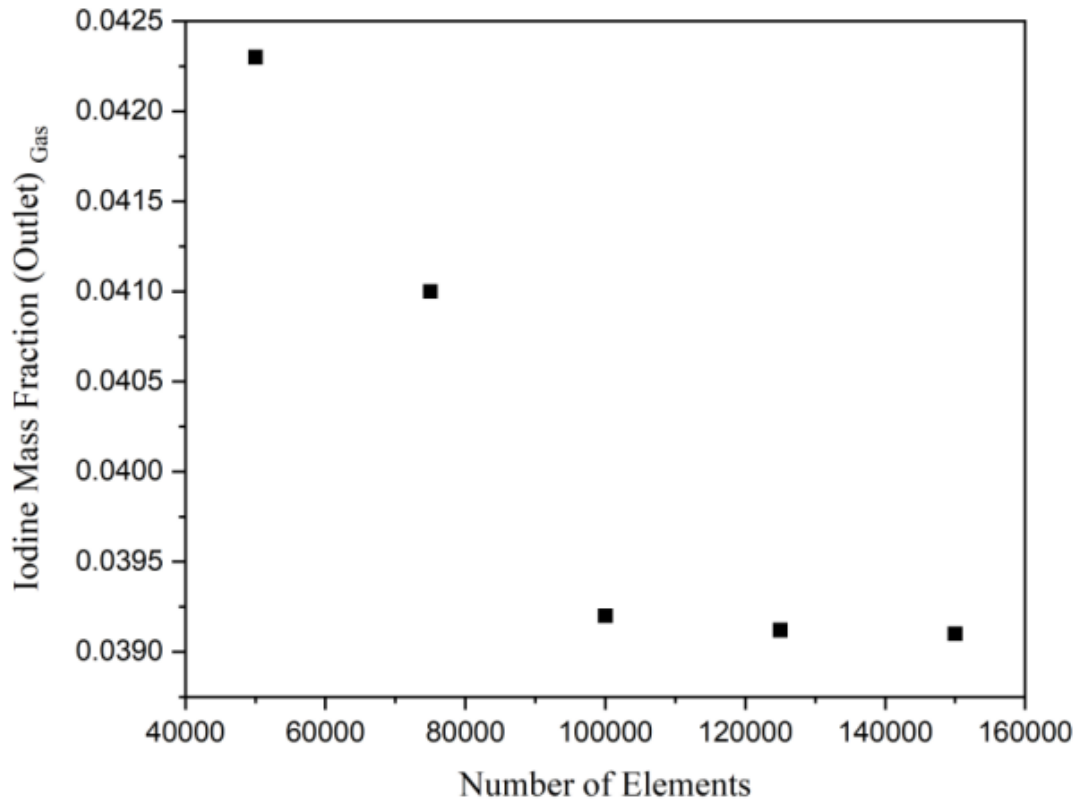

Fig. 4.5 Testing grid independence

4.2. Boundary Conditions

The liquid and gas phase enter through a velocity inlet, while the outlet was taken as a pressure inlet. Both the gas and liquid streams were given a fixed starting temperature of 300 K. The simulation was run for three different gas flow rates, 240 m³/hr, 290 m³/hr, and 340 m³/hr, for validation with experimental results reported by Ali et al. [1]. These flow rates were converted into velocity for inputting into the solver.

On the other hand, the liquid velocity was kept fixed at 2.21 m/s, and all other parameters like initial Iodine mass fraction and Thiosulfate mass fraction were kept constant to accurately study the behavior of gas flow rate. The walls of the venturi scrubber were given a no-slip condition and isothermal boundary condition.

4.3. Coupling the Chemical Reaction with Mass Transfer

By default, iodine, thiosulfate, iodide, and tetrathionate are not present in ANSYS Fluent materials directory. The following custom materials as shown in table 4.1 were defined in Ansys Fluent and their respective properties like Density, Viscosity, and Molecular Weight were taken from literature:

Table 4.1 Custom species defined in Ansys Fluent

Material Name	Chemical Formula	Molecular Weight (kg/kg-mol)	Density (kg/m3)	Viscosity (kg/m-s)
Iodine	I_2	253.8	11.27	0.0022
Thiosulfate	$S_2O_3^{2-}$	112.0	998.2	0.001003
Iodide	I^-	126.9	998.2	0.001003
Tetrathionate	$S_4O_6^{2-}$	224.0	998.2	0.001003

Two phases were defined in ANSYS FLUENT. The primary phase being the gas-phase and the secondary phase being the liquid phase. The gas phase comprises of air and iodine. The liquid phase comprises of water, iodine, thiosulfate, iodide, tetrathionate. The reason for keeping the density and viscosity of thiosulfate, iodide and tetrathionate same as that of water as shown in table 3 is that the concentration of these species is negligible as

37

compared to the amount of water in liquid phase. The surface tension between the two phases was given a constant value of 0.072 N/m.

A user-defined function was written in C++ to couple the mass transfer of Iodine and its simultaneous consumption due to reaction with Thiosulfate based on the theoretical model of Iodine reaction developed by Ling et al. [2].

The Eulerian multiphase model was applied with the energy equation set to on. The First Order Upwind Scheme was used to solve energy equations, turbulence parameters, mass fractions of species, and momentum. For pressure-velocity coupling, a Phase Coupled SIMPLE scheme was used. RNG k-ε was selected for turbulence modeling.

Modified HRIC was used for solving the volume fraction equation. A time-step size of 0.01 seconds was applied to the transient state with a total of 5000 timesteps. The output parameters variance was observed, and the simulation was stopped when the variance became negligible.

Previous works in literature, such as those by Ali et al. [3] ignored the effects of the reaction assuming it to be a rapid reaction. A flow chart of the algorithm of the user-defined function (UDF) is shown in figure 4.6:
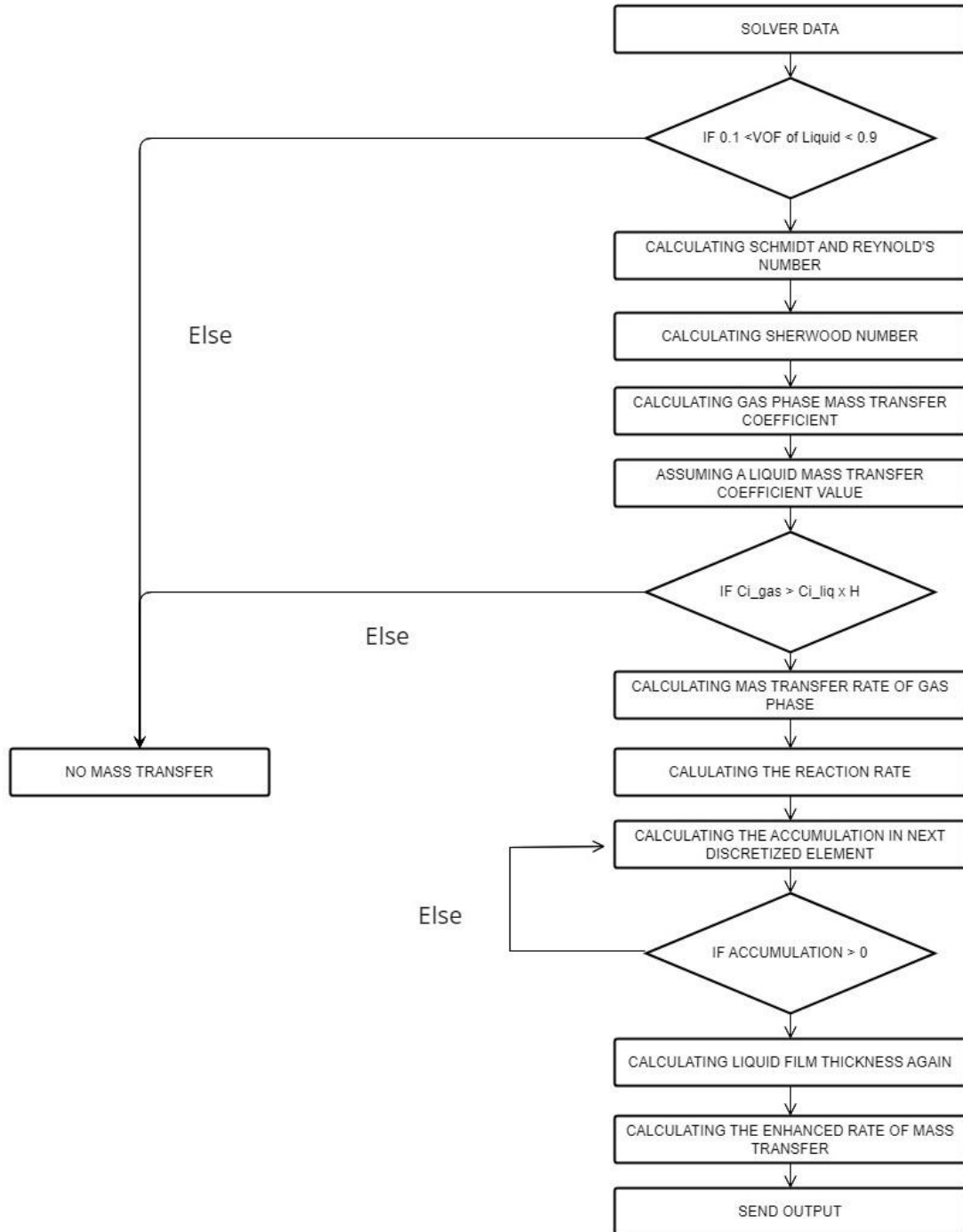
Fig. 4.6 Algorithm for mass transfer coupled with reaction.

Summary

This chapter discusses the CFD methodology that has been used in this study. The Eulerian-Eulerian approach has been used, with RNG k-epsilon turbulence model. The geometry was created in Solidworks and imported in ICEM CFD for meshing. O-rings were generated and parts of the blocks were removed to account for the empty space in the geometry. A range of meshes were generated with varying number of elements and imported in Ansys Fluent for an independence test. The best mesh was selected. A UDF was written in C++ and hooked to Ansys Fluent to model the mass transfer and coupling with chemical reaction.

References

[1]   M. Ali, Y. A. N. Chanqgi, S. U. N. Zhongning, G. U. Haifeng, W. Junlong, and K. Mehboob, "Iodine Removal Efficiency in Non-Submerged and submerged self-priming venturi scrubber," *Nucl. Eng. Technol.*, vol. 45, no. 2, pp. 203–210, 2013.

[2]   G. J. Evans and J. R. Ling, "Enhancement of the interfacial transfer of iodine by chemical reaction," *Can. J. Chem. Eng.*, vol. 78, no. 1, pp. 221–225, 2000.

[3]   M. Ali, C. Yan, Z. Sun, H. Gu, and J. Wang, "Study of iodine removal efficiency in self-priming venturi scrubber," *Ann. Nucl. Energy*, vol. 57, pp. 263–268, 2013.

Chapter 5

Results and Discussion

5.1. Iodine Mass Transfer Rate Enhancement and Model Validation

Previously, Ali et al. [1], Ashfaq et al. [2], and Goel et al. [3], assumed the liquid side film thickness to be negligible for a reaction between iodine and thiosulfate. Hence, the effects of chemical reaction were ignored in calculations obtained in the past studies present in literature and only the gas-side mass transfer coefficient was considered in theoretical calculations and simulations.

However, this reduces the accuracy of the results because the chemical reaction between iodine and thiosulfate greatly affects the mass transfer rate of iodine and its removal efficiency.

The current model combines the effects of the chemical reaction with mass transfer of iodine with the help of a UDF. Results of the simulation showed that the mass transfer rate of Iodine from gas to liquid increased with an increase in the gas flow rate in an almost linear fashion.

This enhancement in the mass transfer rate results in increased removal of Iodine from the gas phase, which can be attributed to the effects of turbulence at higher gas flow rates.
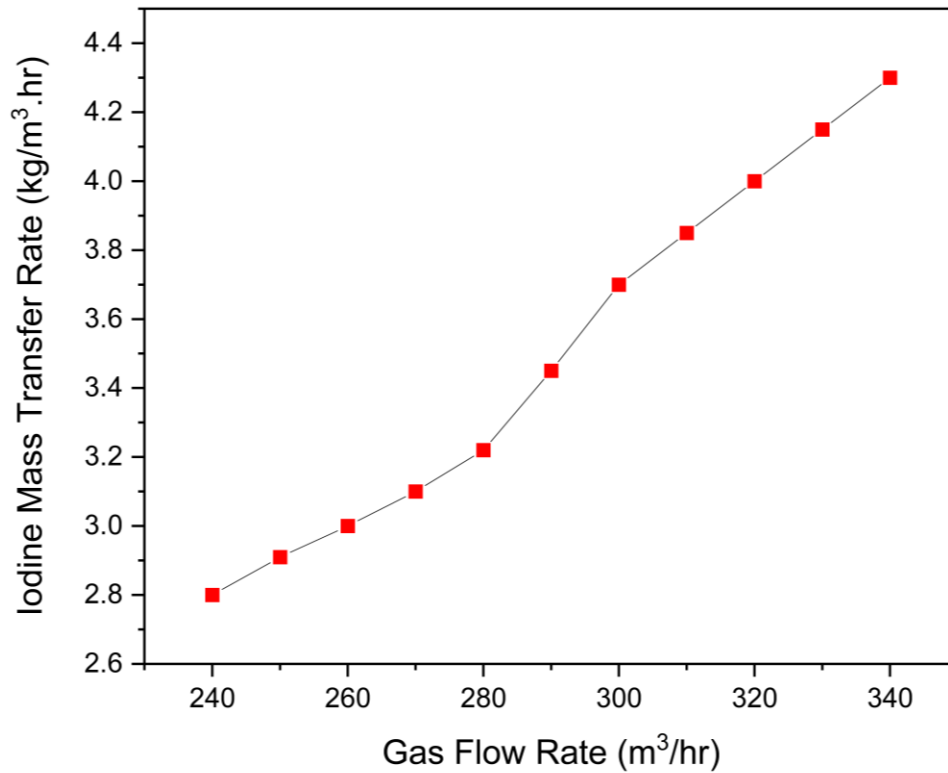
Fig. 5.1 Graph of Iodine's rate of mass transfer against gas flow rate

The Iodine removal efficiency was also found to increase with an increase in the gas flow rate, which is in line with the observations reported in literature.

For qualitative validation, results of the current study were compared with the experiments performed by Ali et al. [1] on a submerged self-priming venturi scrubber.

It was found that the current study accurately predicts the iodine removal efficiency for higher gas flow rates. However, the model also overpredicts the iodine removal efficiency for lower gas flow rates, hence reducing the accuracy in the case of lower gas flow rates.
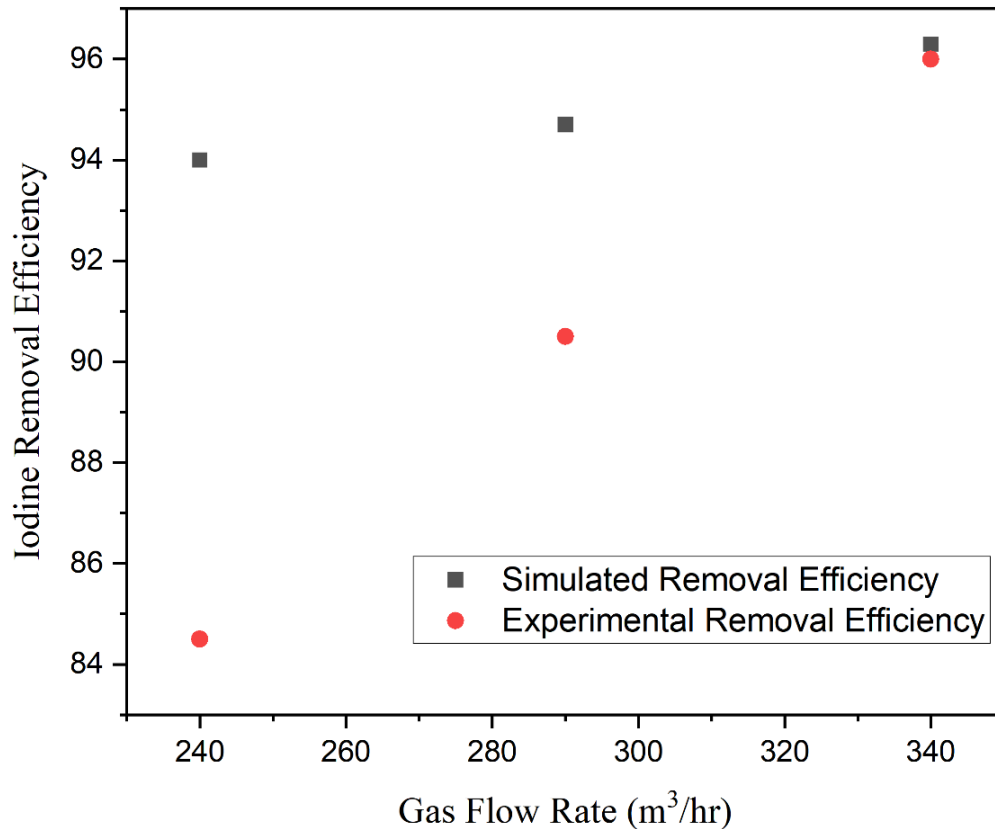
Fig. 5.2 A comparison between graph of simulated and experimental efficiency

The main reason for the discrepancy in results for low gas flow rates is the fact that in a practical experimental setup, the droplet distribution is not perfectly uniform, especially in the case of low flow rates. That is because the liquid primarily disintegrates into tiny droplets due to the incoming force of the high-speed gas. After that, mass transfer and reaction occur with each individual drop of the scrubbing solution.

In practical situations, the droplet size and its distribution tend to vary due to many factors, among which the gas flow rate is a major factor. At higher gas flow rates, the droplet distribution naturally tends to be more uniform and the droplet sizes are smaller in practical scenarios [4], [5].

While the opposite is true for lower gas flow rates. In our CFD setup, we had assumed that droplet distribution is uniform, the droplet diameter to be constant, and the droplets are in perfect spherical shape, to reduce complexities. Hence, the model is more accurate for higher gas flow rates.
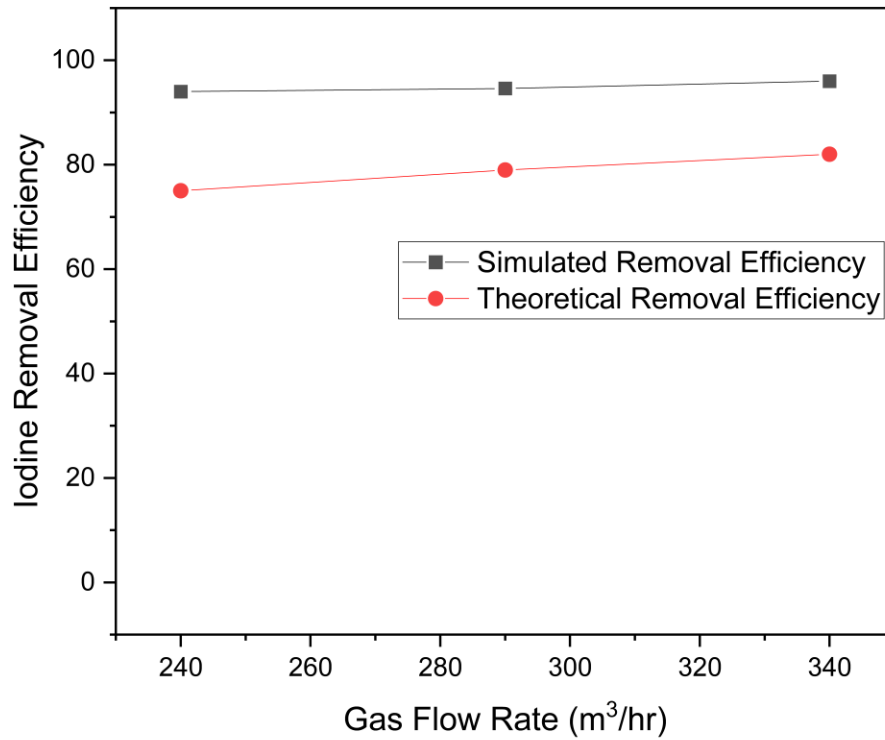
Fig. 5.3 A comparison between graph of simulated and Theoretical efficiency

We also compared our simulated results with the theoretical calculations done by Majid et al. [1] in which only the gas side mass transfer coefficient was used, while the liquid film thickness was considered to be negligible. On average, our calculations through simulation yielded 20% higher iodine removal efficiency after coupling the chemical reaction with mass transfer.
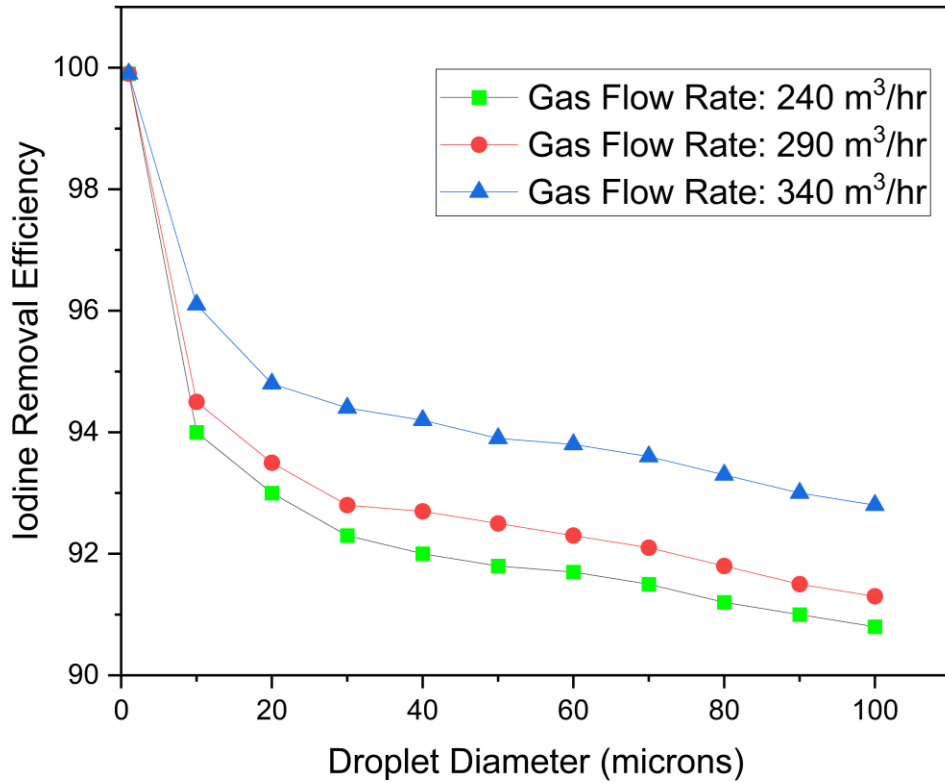
Fig. 5.4 Effect of varying droplet diameter on iodine removal efficiency

The effect of variation of droplet diameter on iodine removal efficiency was also studied. It was found that the efficiency is approximately 99.8% for all gas flow rates when the droplet diameter is set to 1 micron. The prime reason for this behavior is that the resulting liquid side film is so thin, that the rate of mass transfer can be considered instantaneous. This results in rapid mass transfer and hence, a high iodine removal efficiency in light of this model. Consequently, when the droplet diameter is increased, we see a reduction in the iodine's removal efficiency for all gas flow rates. However, at any droplet diameter, the removal efficiency is higher for the higher gas flow rate value.

At a droplet diameter of 10-microns, the efficiency reduces by 6%, 5.5%, and 4% for the gas flow rates of 240 m^3/hr, 290 m^3/hr, and 340 m^3/hr, respectively. Overall, when the droplet diameter was increased to 100 microns, the resulting reduction in efficiency was 9.9%, 8.6%, and 7.1% for the same gas flow rate values, respectively.

46

Hence, as the droplet diameter value approaches 10 microns, we can start seeing noticeable reduction in the iodine removal efficiency. This is simply due to the fact that at this point, the liquid side film starts becoming thicker and hence, the film reduction due to chemical reaction is not rapid anymore.

5.2. Hydrodynamics of Venturi Scrubber

This section presents the effect of inlet gas velocity on the simulation of iodine absorption in a sodium thiosulfate solution inside a venturi scrubber. The gas inlet flow rate was varied from 240 m^3/hr to 340 m^3/hr to study the effect on the hydrodynamics in the venturi scrubber, the compounds formed and consumed due to the reaction, and the enhancement in the rate of mass transfer due to the reaction.

Most of the gas remains concentrated towards the center of the venturi scrubber due to incompressible liquid entering from the sides near the throat section. Furthermore, the gas velocity was found to be the highest near the center of the venturi scrubber and reduced along the throat.
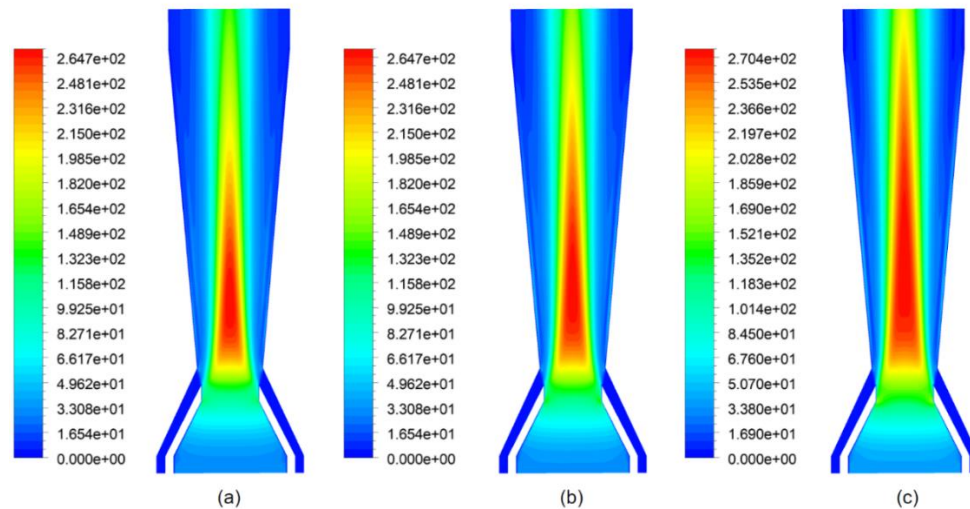

Fig. 5.5 Gas velocity contours at (a) 240 m^3/hr (b) 290 m^3/hr (c) 340 m^3/hr

The velocity of liquid is highest near the center of the venturi scrubber due to a no-slip condition on the inner walls. This causes the liquid to form a stationary layer right alongside the scrubber's inner wall. On the other hand, liquid moves at the highest velocity in the center where the frictional effect from neighboring layers is the lowest.
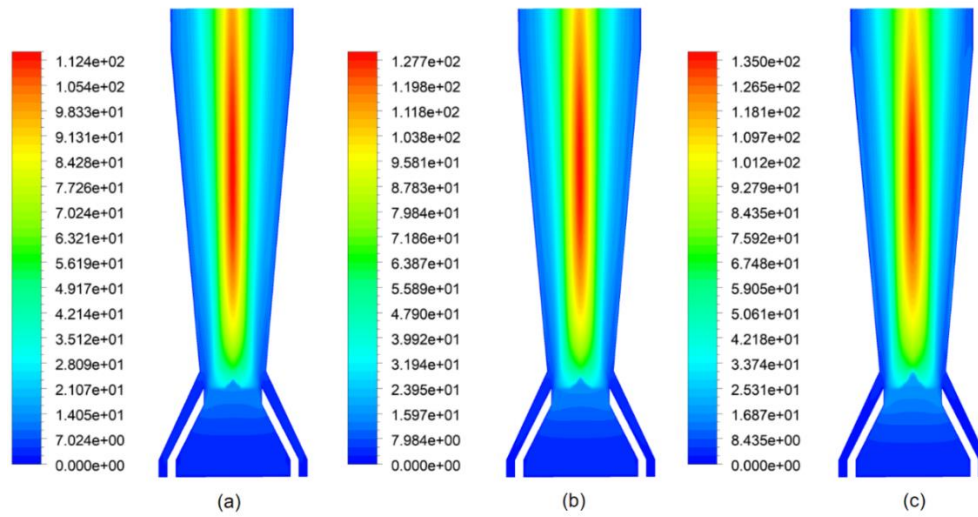
Fig. 5.6 Liquid velocity contours at (a) 240 m^3/hr (b) 290 m^3/hr (c) 340 m^3/hr

5.3. Contours of Iodine Mass Fraction

As the mass flow rate of gas increases, a higher amount of Iodine gets transferred from gas to liquid primarily due to increased turbulence. A high flow rate of gas may reduce the contact time between the gas and liquid droplets. However, the simultaneous consumption of Iodine due to chemical reaction further enhances the mass transfer.
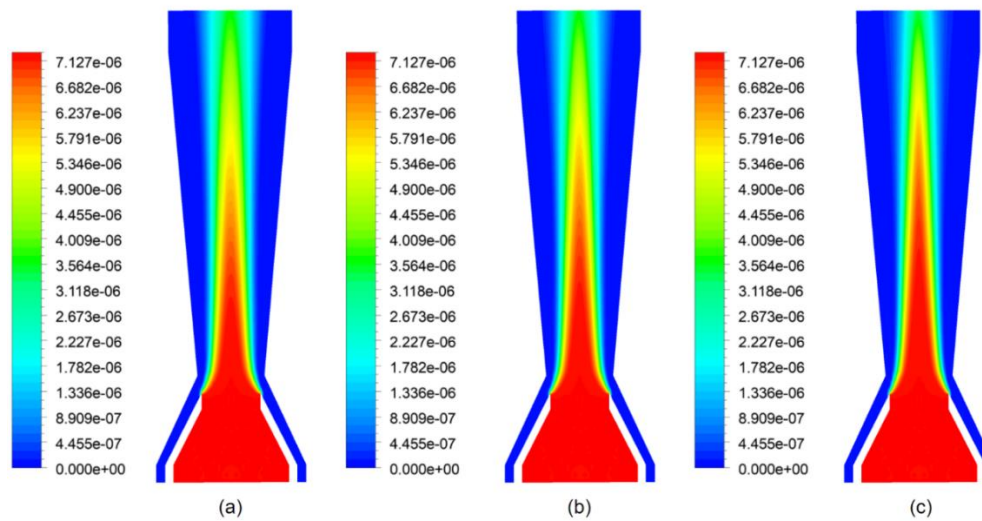

Fig. 5.7 Iodine gas mass fraction contours at (a) 240 m^3/hr (b) 290 m^3/hr (c) 340 m^3/hr

In liquid, the highest amount of Iodine is present near the throat section due to the highest amount of mass transfer occurring in this region. Beyond this point, rapid reaction

between Iodine and Thiosulfate results in the consumption of iodine, producing Iodide and Tetrathionate as byproducts. Overall, with an increase in the gas velocity, a higher amount of iodine was found in the liquid. This happens because of increased turbulent effects allowing higher mass transfer from gas to liquid.
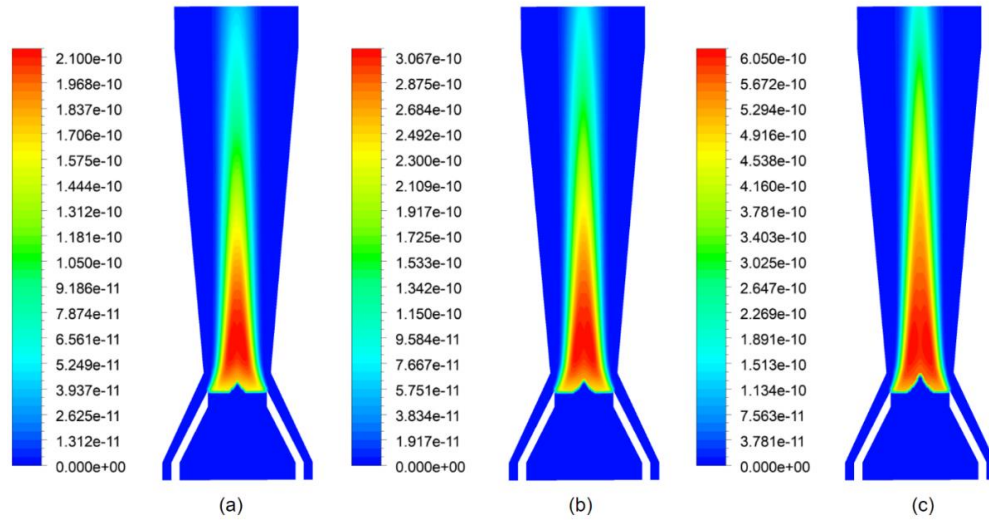

Fig. 5.8 Iodine liquid mass fraction contours at (a) 240 m^3/hr (b) 290 m^3/hr (c) 340 m^3/hr

5.4. Contours of Thiosulfate Mass Fraction

Despite being used up in a reaction with Iodine, there is not enough variation in the mass fraction of thiosulfate present in the liquid. The main reason for this is that the initial mass fraction of Thiosulfate in liquid is significantly higher than the mass fraction of iodine in gas. Even though a little thiosulfate gets consumed in the reaction, thiosulfate's contours do not show any significant variation in the geometry.
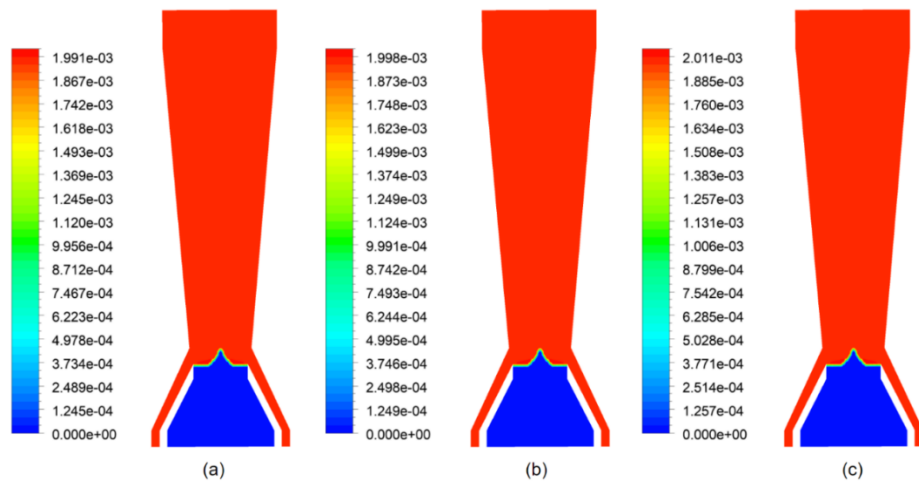
Fig. 5.9 Thiosulfate mass fraction contours at (a) 240 m^3/hr (b) 290 m^3/hr (c) 340 m^3/hr

5.5. Contours of Iodide Mass Fraction

The mechanism of reaction between iodine and sodium thiosulfate first requires the iodine to be converted into an iodide ion, as reported by Scheper et. al [6]. It is noted that the iodide mass fraction in liquid is higher on the outlet for lower gas velocity. As the gas velocity increases, its contour becomes thinner along the length of the scrubber. Overall, the mass fraction of iodide is a lot higher than tetrathionate because of its higher mass produced per unit reactants.
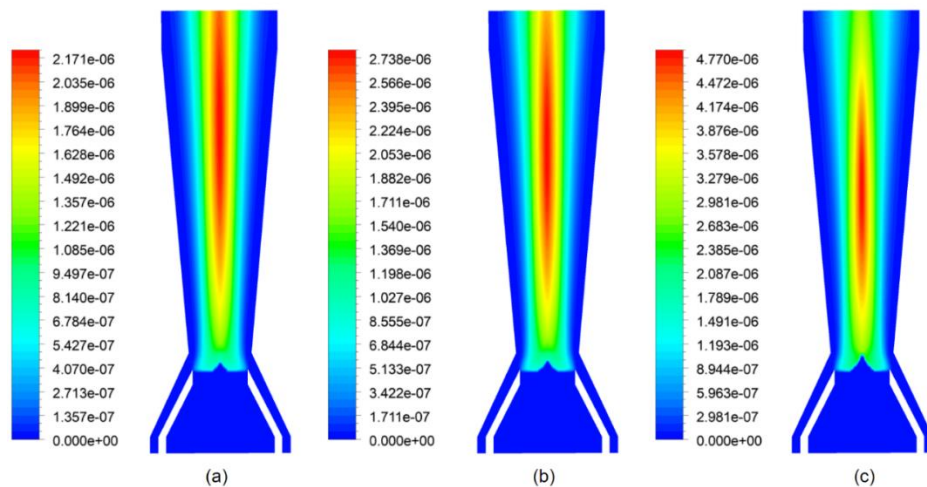

Fig. 6.0 Iodide mass fraction contours at (a) 240 m^3/hr (b) 290 m^3/hr (c) 340 m^3/hr

5.6. Contours of Tetrathionate Mass Fraction

Tetrathionate is a product of the reaction between iodine and sodium thiosulfate. For lower gas velocity, the concentration of tetrathionate appears to be significantly higher around the throat region around which rapid reaction first occurs. With an increase in gas velocity, tetrathionate starts to become more uniformly distributed further downstream as it is quickly carried away due to higher velocity. It can also be noted mass fraction of tetrathionate is lesser than iodide mass fraction since its mass produced per unit reactant is much lesser.
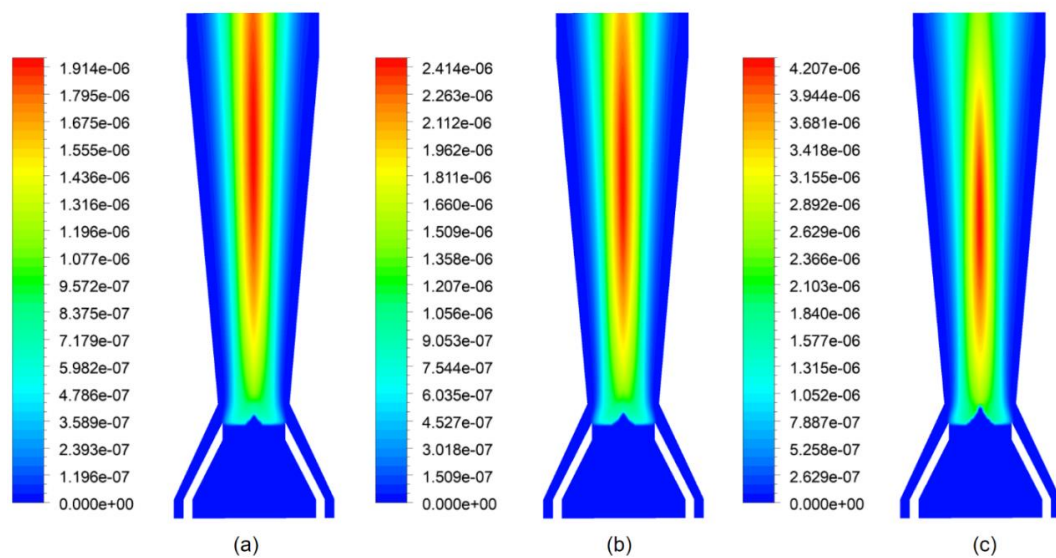

Fig. 6.1 Tetrathionate mass fraction contours at (a) 240 m^3/hr (b) 290 m^3/hr (c) 340 m^3/hr

Summary

In this section, the mass transfer model was validated with the experimental data from the literature. It was found that the model and CFD setup accurately predicts the iodine removal efficiency at high flow rates. However, at low flow rates, the model is less accurate. This is because the current model makes a few assumptions about the droplets. These include a constant diameter, uniform droplet distribution, and perfectly spherical shape. At low flow rates, it has been practically seen that the diameters are larger and less uniform, resulting in less removal efficiency in an experimental scenario. After validation, the contours of different mass species have been presented and analyzed.

References

[1]   M. Ali, Y. A. N. Chanqgi, S. U. N. Zhongning, G. U. Haifeng, W. Junlong, and K. Mehboob, "Iodine Removal Efficiency in Non-Submerged and submerged self-priming venturi scrubber," *Nucl. Eng. Technol.*, vol. 45, no. 2, pp. 203–210, 2013.

[2]   T. Ashfaq *et al.*, "CFD investigation of iodine mass transfer in venturi scrubbing solution of Filtered Containment Venting System," *Prog. Nucl. Energy*, vol. 111, pp. 195–204, Mar. 2019.

[3]   P. Goel, A. Moharana, and A. K. Nayak, "Numerical simulation of injection characteristics, hydrodynamics and absorption of iodine vapour in a venturi scrubber operating in self-priming mode," *Nucl. Eng. Des.*, vol. 341, pp. 360–367, 2019.

[4]   D. Breitenmoser, P. Papadopoulos, T. Lind, and H. M. Prasser, "Droplet size distribution in a full-scale rectangular self-priming Venturi scrubber with liquid film injection," *Int. J. Multiph. Flow*, vol. 142, p. 103694, 2021.

[5]   M. A. M. Costa, P. R. Henrique, J. A. S. Gonçalves, and J. R. Coury, "Droplet size in a rectangular Venturi scrubber," *Brazilian J. Chem. Eng.*, vol. 21, no. 2, pp. 335–343, 2004.

[6]   W. M. Scheper and D. W. Margerum, "Non-Metal Redox Kinetics Reactions of Iodine and Triiodide with Thiosulfate via 12Sz032- and IS203- Intermediates," no. 7, pp. 5466–5473, 1992.

Chapter 6

Conclusion and Future Recommendations

6.1. Conclusion

In this study, a UDF was developed for the mass transfer of Iodine and its simultaneous reaction with thiosulfate inside a venturi scrubber. This UDF was hooked into Fluent, and a CFD analysis was performed.

Contours for the hydrodynamics of the scrubber and mass fractions of gas-liquid components such as iodine, thiosulfate, tetrathionate, and iodide were displayed and analyzed. Mass transfer rate and iodine removal efficiency was then calculated for three different gas flow rates (240, 290, and 340 m^3/hr).

The results of the simulation were compared and validated with the experiments done by Ali et al. [8] on submerged self-priming venturi scrubbers.

1. Iodine removal efficiency was found to increase rapidly as the gas glow rate was increased and was the highest for 340 m^3/hr.
2. For a gas flow rate of 340 m^3/hr, the model predicted iodine removal efficiency with an error deviation of 1.5% in comparison with experimental data. A deviation of 11% was observed for a gas flow rate of 240 m^3/hr and this deviation reduced to less than 2% as the gas flow rate increased.
3. The simulation overpredicted the removal efficiency for gas flow rates lower than 340 m^3/hr due to the assumptions pertaining to droplet size and distribution.
4. The iodine removal efficiency decreases with an increase in the droplet diameter, primarily due to the increase in film thickness and low surface area in contact with gas.
5. For a droplet diameter of 1 micron, the iodine removal efficiency rapidly approaches 99.8% because the liquid side film is so thin that it can be considered

negligible and only the gas side mass transfer coefficient will be sufficient to model the mass transfer accurately.

6. The rate of mass transfer from gas to liquid phase increases as the gas flow rate increases. This directly correlates with an increase in removal efficiency due to higher gas flow rates, which has been observed and reported in the literature.

7. Gas velocity was found to be highest near the center of the throat and decreased along the length of the venturi scrubber, confirming the hydrodynamics of the system.

8. The effect of chemical reaction significantly enhances the mass transfer of iodine and consequently, its removal efficiency due to simultaneous consumption of iodine transferring into the liquid interface.

6.2. Experimental Limitations and Future Recommendations

Some assumptions were made to simply the model for the general case. The droplet distribution in the geometry and droplet sizes were assumed to be perfectly uniform. In practical and experimental setups, the distribution and droplet sizes vary with the gas flow rate.

Furthermore, the droplets were assumed to be in perfectly spherical shape to apply the discretization model. In practical situations, this may not necessarily hold true. It is also important to note that the simulation in this study was performed for a non-submerged venturi scrubber.

Future research can integrate a submerged model where the outlet of the venturi scrubber would become the inlet of a bubble tank, and the mass transfer will be modeled from gas bubbles to bulk fluid, which would further enhance the removal of iodine.

Acknowledgment

Appendix I: Research Article

Title

CFD Analysis of Iodine Mass Transfer Coupled with a Chemical Reaction in a Filtered Containment Venting System

Abstract

Nuclear energy is considered as a zero-emission clean energy source. However, even though it can generate massive amounts of carbon-free electricity, potential accidents in nuclear power plants are a significant threat. Among these, the core meltdown is of significant concern. For environmental safety it is crucial to remove elemental radioactive iodine from flue gases through a system called FCVS (filtered containment venting system). Inside an FCVS, venturi scrubbers are significant, as they help remove the radioactive elements. Many studies have investigated the hydrodynamics of fluids inside venturi scrubbers and modelled the mass transfer of species between gases and scrubbing solutions. However, when it comes to modeling mass transfer coupled with a chemical reaction, the literature is very limited. Previous studies in literature have neglected the effect of chemical reaction on mass transfer. In this study, a UDF was developed to couple mass transfer of iodine and its reaction with Sodium Tetrathionate. The UDF was hooked to a commercial solver called Ansys Fluent, and CFD analysis was performed. The simulations were performed for three different gas flow rates and the resulting mass transfer enhancement was validated with experimental calculations present in the literature. Contours for mass fraction of iodine, thiosulfate, tetrathionate, and iodide along with hydrodynamics of the venturi scrubber were analyzed.

Journal Name

Authors

Muhammad Shummas Humayun, Majid Ali, Muhammad Uzair Qureshi, Muhammad Bilal Khan Niazi, Yan Changqi, Sun Zongning, Gu Hai Feng, Yanmin Zhou